Distribution and Trends of the Cold-Point Tropopause over China from 1979 to 2014 Based on the Radiosonde Dataset

Chaoli Tang[1,2,3], Heli Wei[1,2], Pengfei Wu[1], Congming Dai[1], Wenyue Zhu[1], Ruizhong Rao[1,2], Yingjian Wang[1,2]

[1]Key Laboratory of Atmospheric Composition and Optical Radiation, Anhui Institute of Optics and Fine Mechanics, Chinese Academy of Sciences, Hefei 230031, China;

[2]University of Science and Technology of China, Hefei 230026, China;

[3]Anhui University of Science and Technology, Huainan 232001,China

Corresponding author address: Dr. Heli Wei, Anhui Institute of Optics and Fine Mechanics, Chinese Academy of Sciences, P. O. Box 1125，Hefei, Anhui, China, 230031.

Tel:+86-551-6559153, Fax:+86-551-65591572. Email:hlwei@aiofm.ac.cn .

Key Points

- The significant cooling rate of -0.70K/decade for the T-CPT over China during 1979-2014
- The H-CPT over China is decline trend at low latitude and a uplift trend at high latitude
- Both the variation of H-CPT(T-CPT) and their change rates have spatial distribution characteristics.

Abstract

The Trends of the Cold-Point Tropopause(CPT) are presented using high-resolution radiosonde observations from 77 stations over China during 1979—2014. The latitude region from 18°N to 53°N is divided into 7 latitude zones with every 5° intervals, and the spatial area of 18°N—53°N,75°E—135°E is divided into 27 lattices with 5°×10° grids. The annual-mean values of Height-of-CPT(H-CPT) and Temperature-of-CPT(T-CPT) are obtained. **First**, by using the least squares regression method, it is found that the H-CPT increases with rate of 273m/decade, and overall significant cooling rate of -0.70K/decade for the T-CPT over China. **Then**, the trends and latitude distribution of H-CPT and T-CPT for each latitude zone are reached. The change rates (even the change direction) of H-CPT(H-CPT) show obviously latitude distribution characteristics. The characteristic difference of H-CPT among latitude distribution is reducing year by year, and corresponding T-CTP is enlarging. The H-CPT displays uplift trend between 28°N—53°N latitude region with the positive change rates, and corresponding it has decline trend between 18°N—28°N latitude region with the negative change rates. The change rates of T-CPT are negative values for all latitude zones. **Third**, the spatial(latitude-longitude) distribution of long-term trends of H-CPT(T-CPT) for each grid are obtained. The change rates of H-CPT(T-CPT) are not only dependent on latitude, but also on longitude. **At last**, the spatial structure of annual fluctuation of H-CPT(T-CPT) for each grid are obtained. The fluctuation of standard deviations of T-CPT is not only related to spatial distribution, but also to economic belt of China.

Index Terms and Keywords

Cold-Point Tropopause, Cold-Point Temperature, Cold-Point Height, Long-term trends , Change Rate, Radiosonde dataset

1 Introduction

The cold-point tropopause (CPT), a potentially important indicator of global climate change, is one of the most basic structural features of the earth atmosphere [Xie et al., 2014]. The exchange of air mass, water vapor, trace gas and energy between the troposphere and the stratosphere occurs in the tropopause [Zhou et al. 2001a]. The variation of tropopause structure is closely linked to climate change.

Over the past decades, it has become clear that CPT is an atmosphere layer, rather than a sharp surface, which is located between the troposphere and stratosphere, and it has properties of both the troposphere and stratosphere. Owing to its extreme sensitivity to climate variability and climate change, CPT has attracted widely research interests [Joowan and Son,2012; Kim and Alexander,2015]. The growing evidence from a variety of data sources has suggested that the height of the CPT has increased [Austin and Reichler,2008; Kim et al.,2013], and a cooling trend of the tropical T-CPT in the last decades exists[Zhou et al. 2001b], which is closely associated with tropospheric warming and stratospheric cooling.

The CPT, which is defined as the position of the coldest temperature in the vertical temperature profile between troposphere and stratosphere, is applied in this study for climatological statistics. We attempt to estimate the long-term linear variation trends and spatial distributions for the CPT over the whole China region, using radiosonde observations in IGRA v2beta(IGRA2), which is the beta release of version 2 of the Integrated Global Radiosonde Archive as NCDC's baseline upper-air dataset [Durre, I., 2014]. The IGRA data offer substantially higher vertical resolution than reanalysis products, and have much longer records than GPS radio occultation, thus allowing a more accurate identification of the CPT from a climatic perspective [Feng et al., 2012].

China is vast in territory, which latitude spans about 50°(3°51'N-53°33'N), and longitude spans about 62°(73°33'E-135°05'E). The main regions concentrate in the subtropical and temperate zone. The Qinghai-Tibet Plateau of China, known as the third pole or the roof of the world, has its own unique climate characteristics, its effects on climate is worthy of study [Xu et al., 2013]. With the rapid developing industry, the effects of development on the climate and environmental change within China are also worthy of investigations. The analysis of the temporal and spatial variations of the regional climate in China has important significance for the study of climate change. Radiosonde data is by far the most precise directly atmospheric

sounding data and its time spans decades. Thus, it is optimal data source for CPT research. In this study, the cold point tropopause is determined using sounding temperature profiles, through processing nearly 36 years radiosonde observations from 1979 to 2014 derived from IGRA2 sounding data, the temporal and spatial variation characteristics of the CPT is analyzed over China region.

Section 2 outlines the radiosonde data and the methods of data processing and analysis. Section 3 describes long-term trends and spatial variation of the CPT properties over China. The discussions and brief concluding remarks are given in Section 4.

2 Data and Methodologies

2.1 Data Source

The new beta release of version 2 of the Integrated Global Radiosonde Archive(IGRA2), which is now in the documentation and review phase that is a prerequisite for it to officially replace IGRA1 as NCDC's baseline upper-air dataset, was available to public in the September of 2014[Durre, I., 2014]. The IGRA1 quality assurance procedures can be grouped into seven general categories: fundamental “sanity” checks, checks on the plausibility and temporal consistency of surface elevation, internal consistency checks, checks for the repetition of values, climatologically based checks, checks on the vertical and temporal consistency of temperature, and data completeness checks[Durre et al., 2006, 2008]. Compared to IGRA1, IGRA2 is more soundings, longer records, and methodological changes[Durre, I., 2014]. Quality control algorithms have been applied to remove gross errors. Thus, the data source we used in this investigation is the IGRA2-derived sounding dataset. There are 144 stations over China region in the IGRA2-derived dataset which last from 1956-now in time scale.

2.2 The methods for CPT data processing

In order to study the long term variation trends of CPT over China, the H-CPT and T-CPT are firstly identified for each sounding profile based on the definition of CPT. The T-CPT is the minimum temperature which is determined from each sounding profile. The H-CPT is corresponding minimum height for the T-CTP. Owing to some incorrect CPTs in the sounding profiles, it is necessary to preprocess the radiosonde profiles by carrying out quality control for T-CPT with each sounding profile, and the flow chart of quality control is shown in Fig.1. For all the 2,783,403 sounding profiles with any valid sounding data reports over 144 stations in China in the IGRA2-derived during 1956 to 2014, the following three steps have been carried out.

Firstly, those sounding profiles with the maximum height lower than the level of 150hpa are ignored, as the blue star symbol shown in Fig.2. These cases might be due to the sounding balloon does not reach sufficient height and cannot give an effective judge for T-CPT and H-CPT. **Secondly**, the sounding profiles are ignored when the temperature does not rise above the H-CPT for it is an ineffective record, as the black triangle symbol shown in Fig.2. **Finally**, the red dot symbol as shown in Fig.2 is considered as an effective CPT, and the corresponding effective H-CPT and T-CPT meeting the requirements are saved for the following analysis.

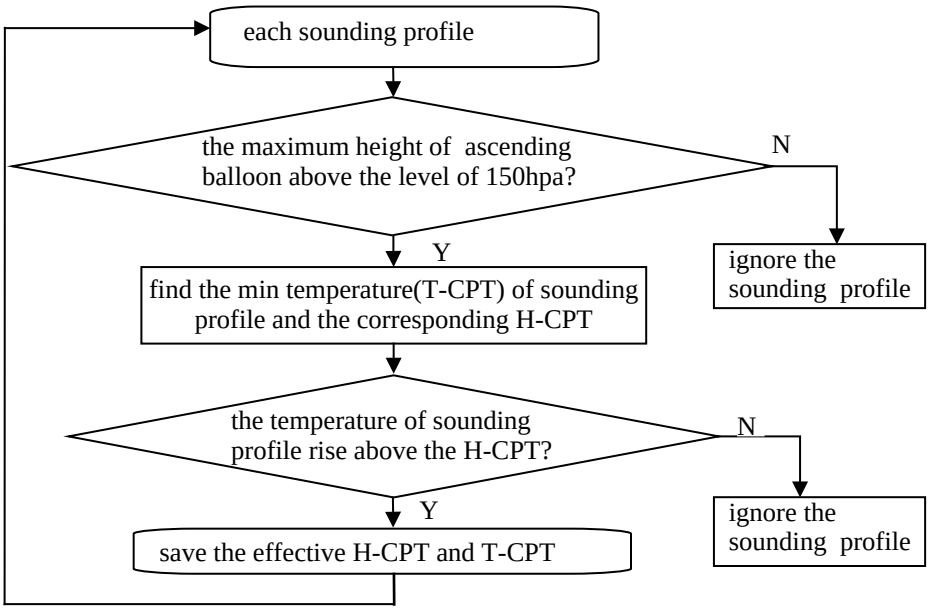

Figure 1. The flow chart of the quality control for the CPT data preprocess: to obtain an effective H-CPT and T-CPT

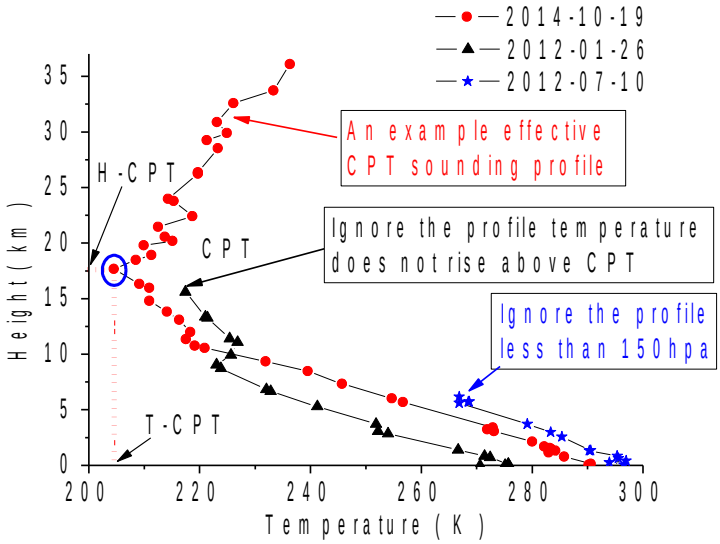

Figure 2. Examples of the CPT data quality control process: three sounding profiles are at 1200 UTC in Beijing (stationID: CHM00054511)

Fig.3a and Fig.3b show the number of sounding stations and distribution of available data in China for each year from 1956 to 2014 in IGRA2-derived dataset. The original data are shown in black triangle, and the effective data after above quality control (Fig.1) for the CPT data processing are shown in red star. After the quality control of CPT, the total number of sounding profiles decreases from the original 2,783,403 to 2,197,989 over China from 1956 to 2014.

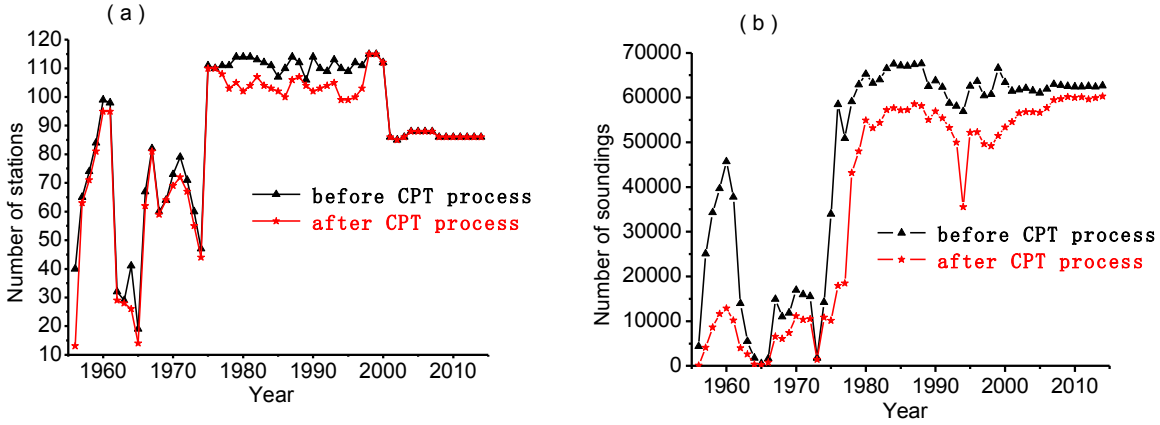

Figure 3. The distribution of available data in China for each year from 1956 to 2014. (a) Number of sounding stations for each year where data are available before CPT quality control process (black triangle) and after CPT quality control process (red star). (b) Number of total sounding profiles for each year where data are available before CPT quality control process (black triangle) and after CPT quality control process (red star).

From the symbol of black triangle shown in Figs.3a and 3b, we can conclude that, before 1978， the number of stations and sounding profiles were relative fewer and rarer in China. After 1978, the number of sounding station is stably more than 85 each year, and the corresponding number of sounding profiles were basically more than 50000 each year. Also found in Fig.3b(red star), the number of effective radiosonde profiles in 1994 is about 1/4 less than that of other years. After analyzing the data source, we find that the radiosonde profiles, which do not meet the quality control of CPT data process requirements(Fig.1), mainly occur in June, July and August of 1994. Thus, in order to reduce the effect on the inter-annual analysis of CPT, the sounding profiles data during 1993.12 to 1994.11 are ignored.

Based on above analysis, there are 77 stations (hereafter S77) sounding data from Chinese 144 stations during 1978.12-2014.11 for this investigation. In the following studies, we take 1978.12-1979.11 as 1979 (winter, spring, summer, autumn), 1979.12-1980.11 as 1980 (winter, spring, summer, autumn), and so on. The purpose of this division is to analyze the impact of seasonal variation on the CPT.

Now, during the period from 1979 to 2014, the total number of 1,709,051 soundings were

left for the S77. According to the relevant literature [Anthes et al., 2008; Son et al., 2011; Xian et al., 2015], there are some abnormal values in H-CPT and T-CPT of 1,709,051 soundings. So it is necessary to remove the abnormal values for H-CPT and T-CPT. In our analyzing, we adopt three times standard deviation threshold to eliminate the abnormal values. With a Statistical analysis, the average value of H-CPT of 1,709,051 soundings is 16.32km, and the corresponding three times standard deviation is 8.37km. The average value of T-CPT of 1,709,051 soundings is 204.46K, and the corresponding three times standard deviation is 22.94K. According to the judgment of three times standard deviation, the values of H-CPT lower than 7.95km (or higher than 24.69km) are identified as abnormal value, and the values of T-CPT lower than 181.52K (or greater than 227.40K) are identified as abnormal value. A total of 5355 sounding profiles are removed in the outside of three times standard deviation for H-CPT and T-CPT, and approximately 99.7 percent of 1,709,051 soundings are normal values.

At last, during the period from 1979 to 2014, the total number of 1,703,696 sounding profiles is adopted in the following investigations for S77. Fig.4a shows the distribution of H-CPT of 1,703,696 soundings in each integer height interval, and Fig.4b shows the distribution of T-CPT of 1,703,696 soundings in each integer temperature interval.

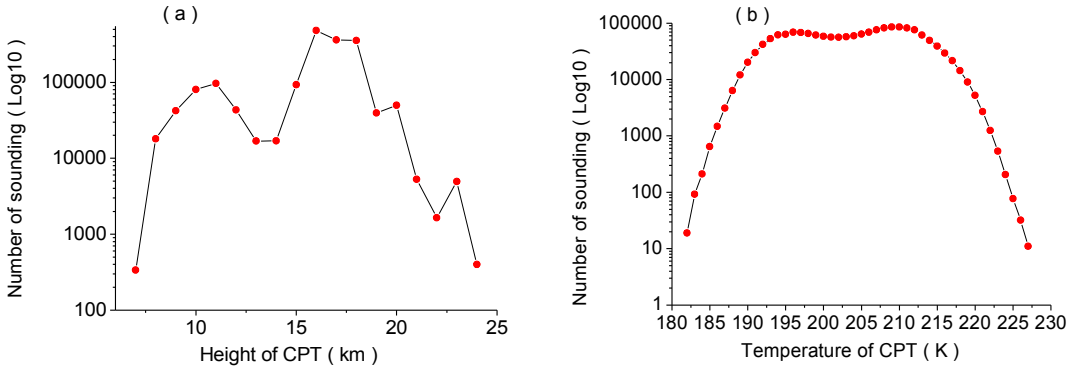

Figure 4. The distribution of H-CPT and T-CPT of 1,703,969 soundings after the abnormal-value-remove. (a) Number of total profiles of H-CPT for each integer height interval. (b) Number of total profiles of T-CPT for each integer temperature interval.

2.3 The methodologies for CPT data analyzing

In order to investigate the seasonal variation trends of CPT properties, we define 4 seasons as: Spring from March to May, Summer from June to August, Autumn from September to November, and Winter from December to February in coming year. For the investigations of the latitude distribution of long-term trends of the CPT properties, we divided the latitude regions from 18°N to 53°N into 7 latitude zones with the interval of 5°, as shown in Fig.5. The average

of H-CPT(T-CPT) for each latitude zone is calculated by the H-CPT(T-CPT) of sounding profiles of all stations within the latitude zone. For the investigations of the spatial (latitude-longitude) structure of the long-term trends of the CPT properties, we divided China region in the area of 18°N—53°N,75°E—135°E into 27 lattice using 5°×10° grids to ensure each grid cell contains a sufficient number of samples as shown in Fig.5. Each cell is signed with the digital number on the top right corner in each grid in Fig.5. The average of H-CPT(T-CPT) over the whole China region is calculated by the corresponding average of 27 grid cells, and the average of H-CPT(T-CPT) for each grid cell is calculated by the H-CPT(T-CPT) of sounding profiles of all stations within the grid cell.

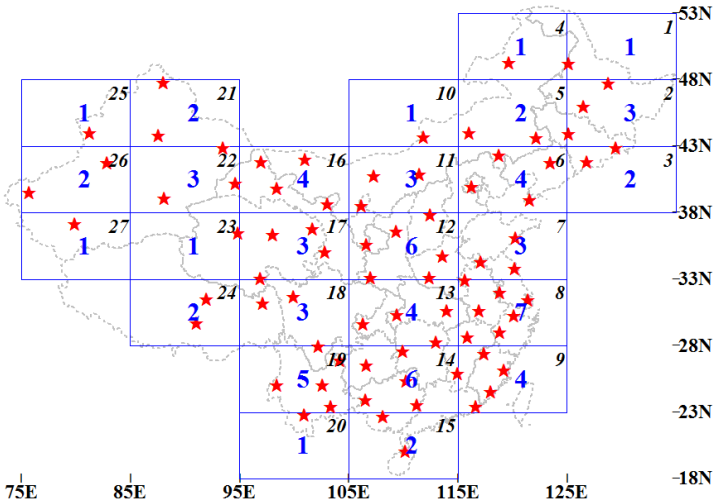

Figure 5. The spatial division and geographic distribution of the 77 stations over China: the red stars mark the location of S77, the blue digital on center in each grid represents the station count of the grid containing, the black digital on the top right corner in each grid represents the number of the grid

In this study, **firstly**, the annual-mean and seasonal average of H-CPT(T-CPT) in the whole China region are calculated by the corresponding average of 27 grid cells. Using the least squares method to calculate the inter-annual variability regression coefficient of H-CPT(T-CPT) over the whole China region, we obtained 10-year-linear-variation-rate of the average temperature and height of CPT. The changing trends of H-CPT(T-CPT) over the whole China region are analyzed. **Then**, the annual-mean and seasonal average of H-CPT(T-CPT) for each latitude zone is calculated and analyzed by using the least squares regression method, and the latitudinal distribution characteristics of H-CPT(T-CPT) are obtained. **Thirdly**, for each grid cell, the annual-mean of the H-CPT(T-CPT) is analyzed using the least squares regression method, and the spatial(latitude-longitude) structure characteristics of 10-year-linear-change-rate of the H-CPT(T-CPT) are obtained. **At last**, using 2014 year's sounding profiles of all stations within

each grid cell, the H-CPT(T-CPT) and their fluctuation are analyzed by the standard deviation method, and the spatial structure of annual fluctuation of H-CPT(T-CPT) is obtained.

3. Results

3.1. Trends of the CPT over the whole China from 1979 to 2014

The average of height and temperature of CPT in the whole China region is calculated by the corresponding average of 27 grid cells. By using the least squares regression method, the long-term evolution trends of H-CPT(T-CPT) are obtained.

Figures 6a and 6b show the annual-mean trends over the whole China for height and temperature of CPT during 1979—2014. The annual-mean of H-CPT(T-CPT) is computed from all grids annual-mean values over China. Figure 6a presents a significant increase in H-CPT over the whole China ranging from 15258m to 16558m during 1979—2014, yielding a net rise of 273m/decade over the 36 years. Figure 6b presents a significant decrease in T-CPT over the whole China ranging from 207.4K to 204.5K during 1979—2014, yielding a net cooling of -0.70K/decade over the 36 years.

Figures 6c and 6d show the seasonal-mean trends for height and temperature of CPT during 1979—2014. The seasonal-mean of H-CPT(T-CPT) is computed from all grids seasonal-mean values over China. It is obviously that the summer's CPT is located highest and coldest than the other seasons' over the whole China. The H-CPT has the trend of increase and the T-CPT has the trend of cooling at all four seasons during 1979—2014, while the variation amplitudes are different for different seasons. Figure 6c presents a significant result that the winter's H-CPT trends is yielding a net rise with a maximum change rate of 398m/decade, while the summer's is minimum with only 86m/decade. The average of H-CPT in summer is the highest, which is over 16km, and the annual change rate is lowest. Compared to the other three seasons, the uplift of summer H-CPT plays a small role in the region of the whole China. Through the correlation analysis, the correlation coefficients of annual trends of H-CPT between the annual-mean and each of the four seasons(Winter, Spring , Summer , Autumn) in the whole China are as following: 0.90,0.90,0.57 and 0.51, respectively. Combined with figure 6c, it can be concluded that the uplift of H-CPT in China region is mainly due to the uplift during winter and spring.

From Fig.6d, it can be seen that T-CPT has an overall cooling trend at all four seasons during 1979—2014, and the largest change rate occurs in winter with the change rate of -0.78K/decade, and the smallest is in autumn with -0.60K/decade. The differences of variation

amplitudes among four seasons are small. The average of T-CPT is lowest in summer and highest in winter, which is showed in Fig.6d. Through the correlation analysis, the correlation coefficient of annual trends of T-CPT between the annual-mean and each of the four seasons(Winter, Spring, Summer, Autumn) in the whole China are as following: 0.85,0.92,0.91 and 0.86, respectively. In conjunction with Fig.6d, it can be drawn that the annual cooling trends of T-CPT of the four seasons have the nearly same role on the annual cooling trend of T-CPT in the whole China region. This suggests that the seasonal cycle of CPT properties is likely modulated by large-scale processes rather than small-scale local processes. In fact, it is known that seasonality in the tropical lower stratosphere is largely controlled by upwelling driven by wave forcing in the extratropical lower stratosphere. The upwelling is stronger during summer than winter, resulting in higher H-CPT and colder T-CPT in summer.

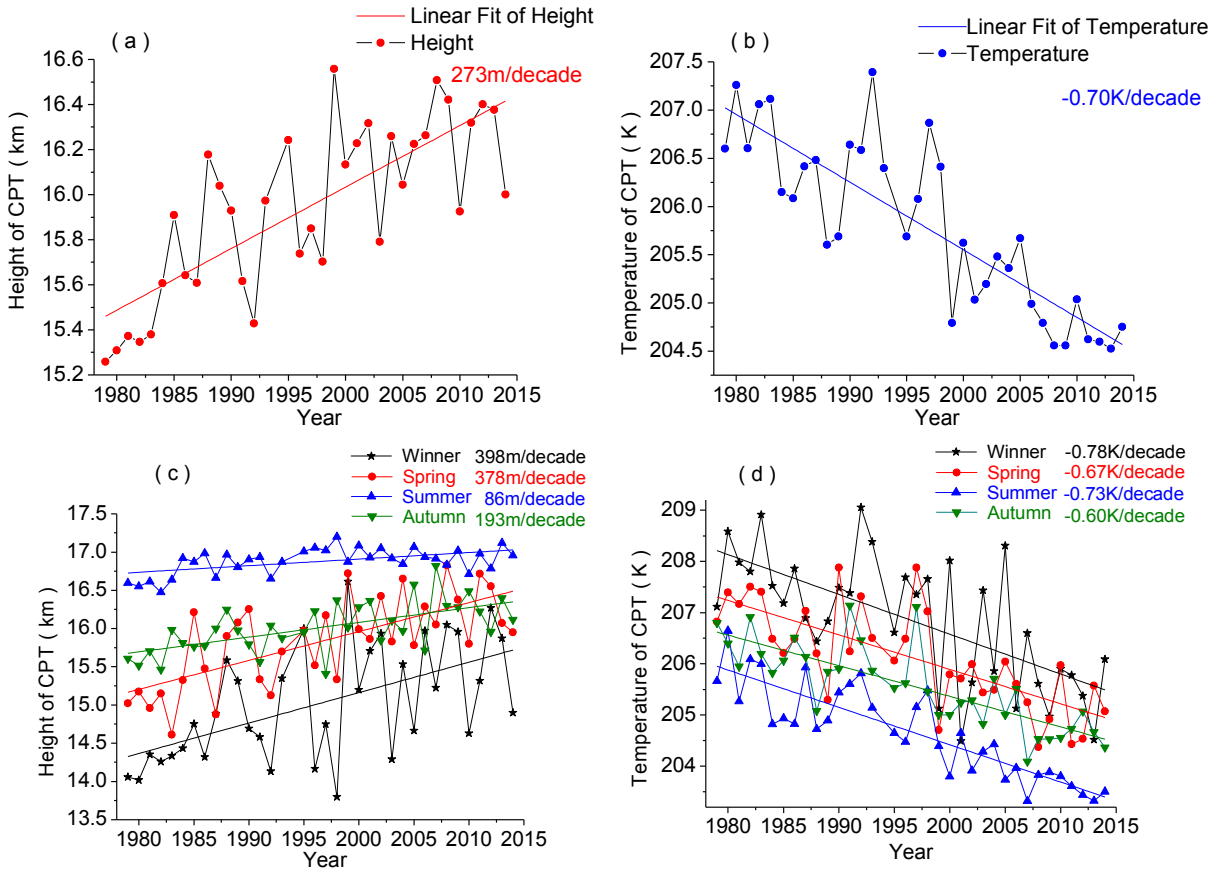

Figure 6. The average variability in height and temperature of CPT. The solid lines are the corresponding linear trends during 1979—2014 with a least square procedure. The change rates are shown at the right-top of each diagram. (a)The annual-mean trends of H-CPT; (b) The annual-mean trends of T-CPT; (c) The seasonal-mean trends of H-CPT; (d)The seasonal-mean trends of T-CPT.

3.2. Latitudinal distribution of the trends of CPT from 1979 to 2014

In order to study the latitude distribution of long-term trends of the CPT properties, the

annual-mean and seasonal-mean of H-CPT(T-CPT) for each latitude zone is calculated by the H-CPT(T-CPT) of sounding profiles of all stations within the latitude zone. Fig.7a (b) shows the annual-mean of H-CPT(T-CPT) for each 5° latitude zone. Fig.8 (also Fig.10) shows the seasonal-mean of H-CPT (T-CPT) for each latitude zone. By using the least squares regression method, the latitudinal distribution characteristics of the change rate of H-CPT(T-CPT) are obtained. Fig.7c (Fig.7d) shows the 10-year-change-rate of H-CPT (T-CPT) for each latitude zone. Fig.9 (also Fig.11) shows the 10-year-change-rate of H-CPT (T-CPT) in different seasons for each latitude zone.

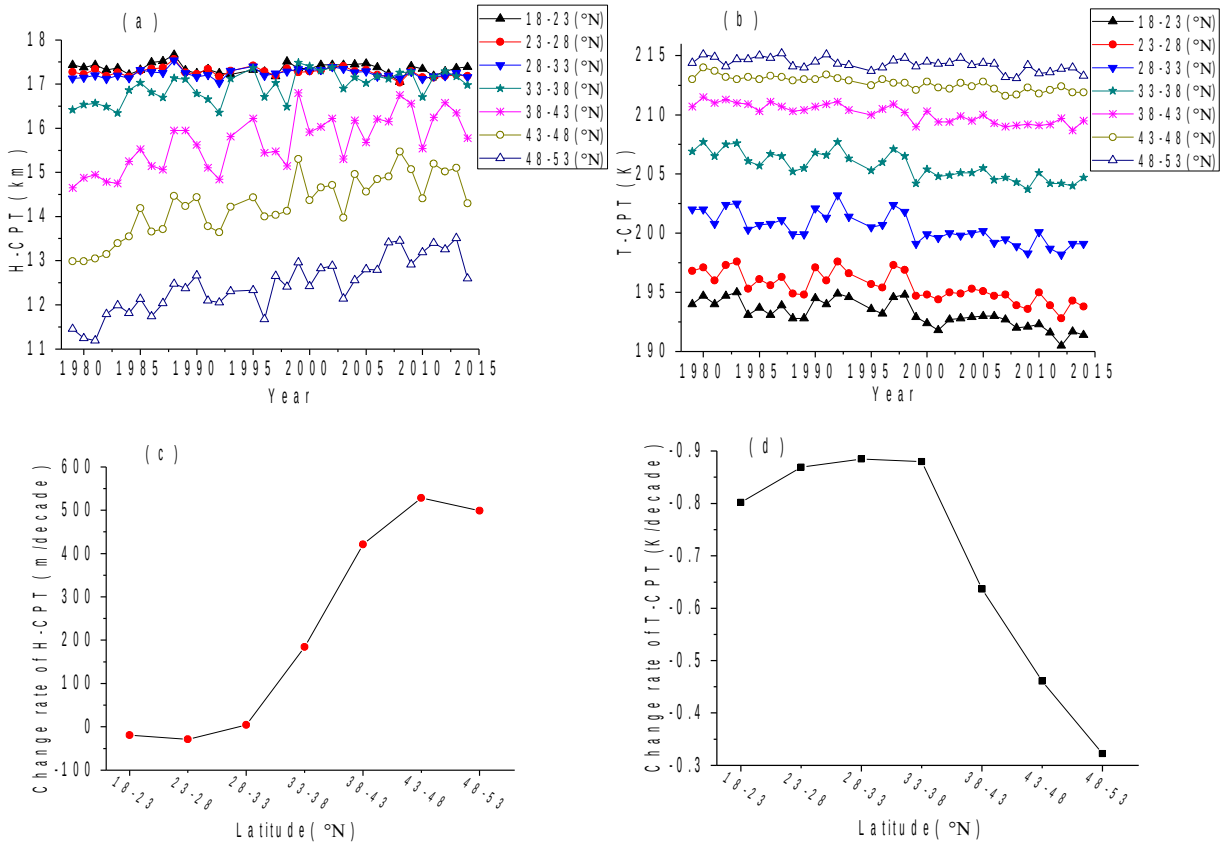

Figure 7. Latitudinal distribution of the annual-mean trends for CPT with the interval of 5° during 1979—2014. (a)The annual-mean trends of H-CPT with respect to soundings in each latitude zone; (b) The annual-mean trends of T-CPT with respect to soundings in each latitude zone; (c) Latitudinal distribution of the 10-year-change-rate for H-CPT; (d) Latitudinal distribution of the 10-year-change-rate for T-CPT

Figures 7a and 7b show the annual-mean trends in height and temperature of CPT for each latitude zone during 1979—2014. From Fig.7a, the H-CPT gradually decreases with the increase of latitude. But in low latitude zones (18°N—33°N) over China, the latitude distribution characteristics of H-CPT is not obviously, and the inter-annual variability is small, and the annual-mean trends of H-CPT are relatively stable during 1979—2014. Conversely, in high

latitude zones (33°N—53°N) over China, the latitude distribution characteristics of H-CPT is remarkable, the inter-annual variability is large. In conjunction with Fig.7c, the uplift trends of H-CPT gradually increase with the increase of latitude within 28°N—48°N latitude zones during 1979—2014. From Fig.7b, the T-CPT gradually increases with the increase of latitude. We can see that the latitude distribution characteristics of T-CPT are obviously. In low latitude zones over China, the inter-annual variability is large, and the corresponding inter-annual variability is small in high latitudes zones. In conjunction with Fig.7d, the cooling trends of T-CPT gradually decrease with the increase of the latitude within 28°N—53°N latitude zones. On the whole, the T-CPT has the cooling trend in each latitude zone, and the larger cooling trend occurs in low latitude zones.

Figures 7c shows the latitude distribution characteristics of the 10-year-linear-change-rate of H-CPT during 1979—2014. From Fig.7c, it can be seen that the change rates (even the change direction) of H-CPT show obviously latitude distribution characteristics. By and large, the change rate of H-CPT decreases from high latitude to low latitude with the change rates vary from positive 499m/decade in high latitude zone (48°N—53°N) to negative -19m/decade in low latitude zone (18°N—23°N). The H-CPT has a uplift trend between 28°N—53°N latitude region with the change rates vary from the minimum 4m/decade in 28°N—33°N latitude zone to 499m/decade in 48°N—53°N latitude zone, the maximum uplifting rate 529m/decade occurs in 43°N—48°N latitude zone. On the contrary, within the low latitude zones, the H-CPT has decline trend between 18°N—23°N latitude zone with -19m/decade and between 23°N—28°N latitude zone with -29m/decade. The decline trend of H-CPT at low latitude was not reported in the previous literature. Combined with Fig.7a, it can be concluded that the annual-mean difference of H-CPT between low-latitude and high-latitude shrinks year by year. Thus, the latitude distribution characteristic of H-CPT reduces year by year. The phenomenon that H-CPT is becoming closer from high latitude to low latitude was not reported before.

Figures 7d shows the latitude distribution characteristics of the 10-year-linear-change-rate of T-CPT during 1979—2014. From Fig.7d, it can be seen that the change rates of T-CPT show obviously latitude distribution characteristics. Basically, the change rate of T-CPT increases from high latitude to low latitude with the change rates vary from the minimum cooling -0.32K/decade in high latitude zone(48°N—53°N) to -0.80K/decade in low latitude zone (18°N—23°N), and the maximum cooling rate -0.89K/decade occurs in latitude zone (28°N—33°N).

The T-CPT has a cooling trend for all latitude zones. In conjunction with Fig.7b, it can be drawn that the annual-mean difference of T-CPT between low-latitude and high-latitude expands year by year. Thus, the latitude distribution characteristic of T-CPT enlarges year by year. The phenomenon that the difference of T-CPT between high latitude and low latitude is becoming larger gradually was not reported before.

In the following section, we will focus on the seasonal statistics of the H-CPT for each latitude zone for further discussion the distribution and the seasonal-mean variation of H-CPT at seven latitude zones over China. Smooth-averaging with time series from original sounding profiles of all stations within each latitude zone to reduce the noises and increase the statistical significance, the seasonal-mean of the H-CPT are analyzed for the seven latitude zones. Fig.8 shows the average of H-CPT in different seasons for each latitude zone during 1979—2014. The H-CPT shows strong seasonal variation, and the latitude distribution characteristics of H-CPT are gradually obvious in accordance with the seasonal order: winter, spring, autumn, summer. Fig.9 shows the 10-year-change-rate of H-CPT in different seasons for each latitude zone.

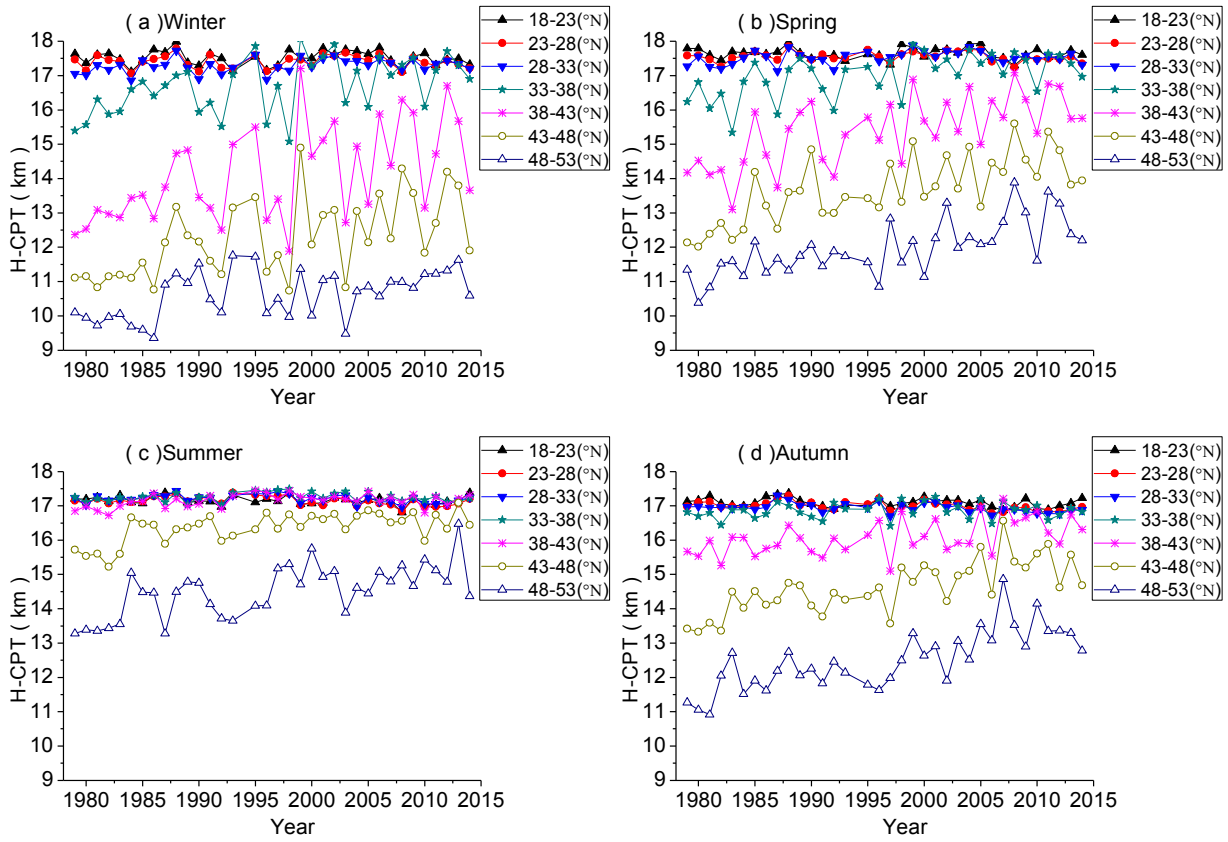

Figure 8. Latitudinal distribution of the seasonal-mean trends for H-CPT in each latitude zone during 1979—2014; (a) Winter; (b) Spring; (c) Summer; (d) Autumn

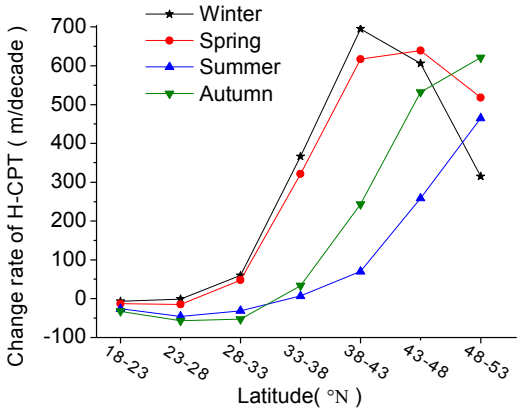

Figure 9. Latitudinal distributions of the 10-year-change-rate of H-CPT with the interval of 5° for four seasons

From Fig.8a, the average of H-CPT in winter exhibits the largest variation amplitudes ranging from 9.4km to 17.8km, and the average of winter's H-CPT gradually decreases with the increase of latitude. In low latitude zones (18°N—33°N), the latitude distribution characteristics of winter's H-CPT is not obviously, and the inter-annual variability is small, and the annual-mean trends of winter's H-CPT are relatively stable during 1979—2014. Conversely, in high latitude zones (33°N—53°N), the latitude distribution characteristics of winter's H-CPT is remarkable, the inter-annual variability is large. In conjunction with Fig.9, the uplift trends of H-CPT in winter gradually increase with the increase of latitude within 28°N—43°N latitude zone during 1979—2014.

From Fig.8b, the average of H-CPT in spring exhibits the larger variation amplitudes ranging from 10.4km to 18km. The latitude distribution characteristics of spring's H-CPT is not obviously within 18°N—33°N latitude zones, and corresponding it is remarkable within 33°N—53°N latitude zones. In conjunction with Fig.9, the uplift trends of H-CPT in spring gradually increase with the increase of latitude within 28°N—48°N latitude zones during 1979—2014.

From Fig.8c, the average of H-CPT in summer exhibits the smallest variation amplitudes ranging from 13.3km to 17.4km. The latitude distribution characteristics of summer's H-CPT is not obviously within 18°N—43°N latitude zones, and the inter-annual variability is small, and the annual-mean trends of summer's H-CPT are relatively stable during 1979—2014. Conversely, the latitude distribution characteristics of summer's H-CPT is remarkable within 43°N—53°N latitude zones, the inter-annual variability is large. In conjunction with Fig.9, the uplift trends of H-CPT in summer gradually increase with the increase of latitude within 33°N—53°N latitude zone during 1979—2014.

From Fig.8d, the average of H-CPT in autumn exhibits the smaller variation amplitudes ranging from 10.9km to 17.4km. The latitude distribution characteristics of autumn's H-CPT is not obviously within 18°N—38°N latitude zones, and corresponding it is remarkable within 33°N—53°N latitude zones. In conjunction with Fig.9, the uplift trends of H-CPT in autumn gradually increase with the increase of latitude within 33°N—53°N latitude zone during 1979—2014.

From Fig.9, it can be seen that the 10-year-change-rates (even the change direction) of H-CPT in different seasons show obviously latitude distribution characteristics. By and large, the 10-year-change-rates of H-CPT increases from low latitude to high latitude for each season. The black star symbol shown in Fig.9 is 10-year-change-rates for winter's average of H-CPT during 1979—2014. The winter's H-CPT has a uplift trend between 28°N—53°N latitude region with the change rates vary from the minimum 59m/decade in 28°N—33°N latitude zone to 315m/decade in 48°N—53°N latitude zone, the maximum uplifting rate 695m/decade occurs in 38°N—43°N latitude zone. On the contrary, at the low latitude zones, the winter's H-CPT has a decline trend between 18°N—28°N latitude region. The red dot symbol shown in Fig.9 is 10-year-change-rates for spring's average of H-CPT during 1979—2014. The spring's H-CPT has a uplift trend between 28°N—53°N latitude region with the change rates vary from the minimum 48m/decade in 28°N—33°N latitude zone to 518m/decade in 48°N—53°N latitude zone, the maximum uplifting rate 639m/decade occurs in 43°N—48°N latitude zone, and corresponding it has a decline trend between 18°N—28°N latitude region. The blue upper triangle symbol shown in Fig.9 is 10-year-change-rates for summer's average of H-CPT during 1979—2014. The summer's H-CPT has a uplift trend between 33°N—53°N latitude region with the change rates vary from the minimum 7m/decade in 33°N—38°N latitude zone to the maximum 465m/decade in 48°N—53°N latitude zone, and corresponding it has a decline trend between 18°N—33°N latitude region. The olive lower triangle symbol shown in Fig.9 is 10-year-change-rates for autumn's average of H-CPT during 1979—2014. The autumn's H-CPT has a uplift trend between 33°N—53°N latitude region with the change rates vary from the minimum 33m/decade in 33°N—38°N latitude zone to the maximum 621m/decade in 48°N—53°N latitude zone, and corresponding it has a decline trend between 18°N—33°N latitude region. The largest uplift of H-CPT occurs in winter within 38°N—43°N mid-latitude zone. Combined with Fig.8 and Fig.9, it can be concluded that the differences of H-CPT between low-latitude and high-latitude shrinks

year by year for each season.

In the following section, we will focus on the seasonal statistics of the T-CPT for each latitude zone for further discussion the distribution and the seasonal-mean variation of T-CPT at seven latitude zones over China. Fig.10 shows the average of T-CPT in different seasons for each latitude zone during 1979—2014. The latitude distribution characteristics of T-CPT are very obviously in each season, and the T-CPT gradually increases with the increase of latitude. Fig.11 shows the 10-year-change-rate of T-CPT in different seasons for each latitude zone.

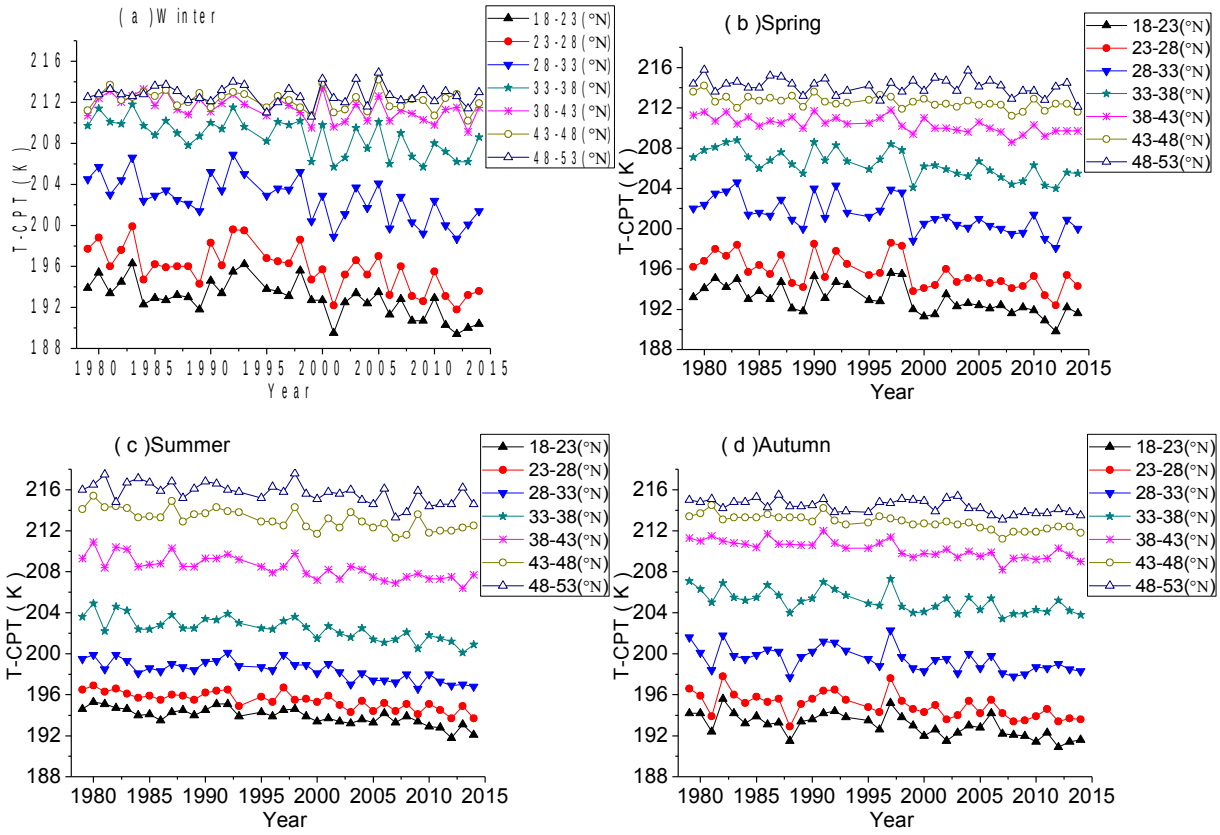

Figure 10. The latitudinal distribution of the seasonal-mean trends for T-CPT in each latitude zone during 1979—2014; (a) Winter; (b) Spring; (c) Summer; (d) Autumn

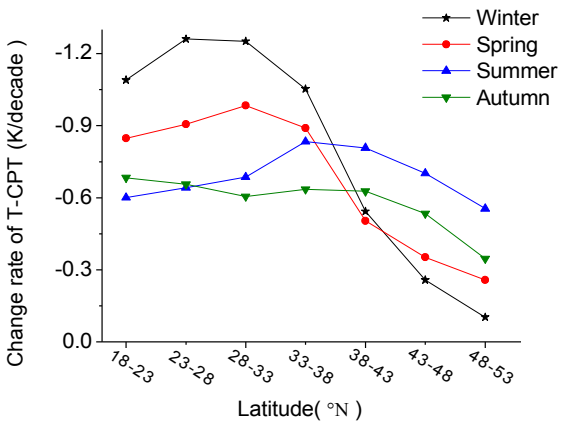

Figure 11. The latitudinal distribution of the 10-year-change-rate of T-CPT with the interval of 5° for four seasons

From Fig.10a, in high latitude zones (38°N-53°N), the latitude distribution characteristics of winter's T-CPT is not obviously, and the annual-mean trends of winter's T-CPT are relatively stable during 1979-2014. Conversely, in low latitude zones (18°N-38°N), the latitude distribution characteristics of winter's T-CPT is remarkable, the inter-annual variability is large. From Fig.10b (10c or 10d), the average of T-CPT in spring(summer or autumn) gradually increases with the increase of latitude, and the latitude distribution characteristics of T-CPT in spring(summer or autumn) are remarkable.

Fig.11 shows the latitude distribution characteristics of the 10-year-linear-change-rate of T-CPT in different seasons during 1979—2014. On the whole, the T-CPT in each season (spring, summer, autumn and winter) has the cooling trend for all latitude zones during 1979-2014. The black star symbol shown in Fig.11 is 10-year-change-rates for winter's average of T-CPT during 1979-2014, it can be seen that the change rates of winter's T-CPT show obviously latitude distribution characteristics. Basically, the change rate of winter's T-CPT increases from high latitude to low latitude with the change rates vary from the minimum cooling rate -0.10K/decade in high latitude zone(48°N—53°N) to -1.09K/decade in low latitude zone (18°N—23°N), and the maximum cooling rate -1.26K/decade occurs in latitude zone (23°N—28°N). In conjunction with Fig.10a, it can be drawn that the difference of winter's T-CPT between low-latitude and high-latitude expands year by year. The red dot symbol in Fig.11 is 10-year-change-rates for spring's average of T-CPT during 1979-2014, it can be seen that the change rates of spring's T-CPT show obviously latitude distribution characteristics. By and large, the change rate of spring's T-CPT increases from high latitude to low latitude with the change rates vary from the minimum cooling rate -0.26K/decade in high latitude zone(48°N—53°N) to -0.85K/decade in low latitude zone

(18°N—23°N), and the maximum cooling rate -0.98K/decade occurs in latitude zone (28°N—33°N). In conjunction with Fig.10b, it can be concluded that the latitude distribution characteristic of the spring's T-CPT enlarges year by year. The blue upper triangle symbol shown in Fig.11 is 10-year-change-rates for summer's average of T-CPT during 1979-2014, it can be seen that the change rates of summer's T-CPT are relatively stable for all latitude zones. The minimum cooling rate -0.55K/decade occurs in high latitude zone(48°N—53°N), and the maximum cooling rate -0.83K/decade occurs in latitude zone (33°N—38°N). The olive lower triangle symbol shown in Fig.11 is 10-year-change-rates for autumn's average of T-CPT during 1979-2014, it can be seen that the change rates of autumn's T-CPT show obviously latitude distribution characteristics. Basically, the change rate of autumn's T-CPT increases from high latitude to low latitude with the change rates vary from the minimum cooling rate -0.35K/decade in high latitude zone(48°N—53°N) to the maximum cooling rate -0.68K/decade in low latitude zone (18°N—23°N). In conjunction with Fig.10d, it can be drawn that the difference of autumn's T-CPT between high latitude and low latitude is becoming larger year by year.

3.3. Spatial (latitude—longitude) structure of the change rate of CPT during 1979-2014

In order to study the spatial (latitude-longitude) structure of long-term trends of the CPT properties, the annual-mean of the H-CPT (T-CPT) is analyzed using least squares regression method for each grid cell. The spatial distribution of the 10-year-linar-change-rate of H-CPT and T-CPT are obtained. Fig.12 and Fig.13 show the 10-year-linear-change-rate of H-CPT and T-CPT for each grid over 1979—2014.

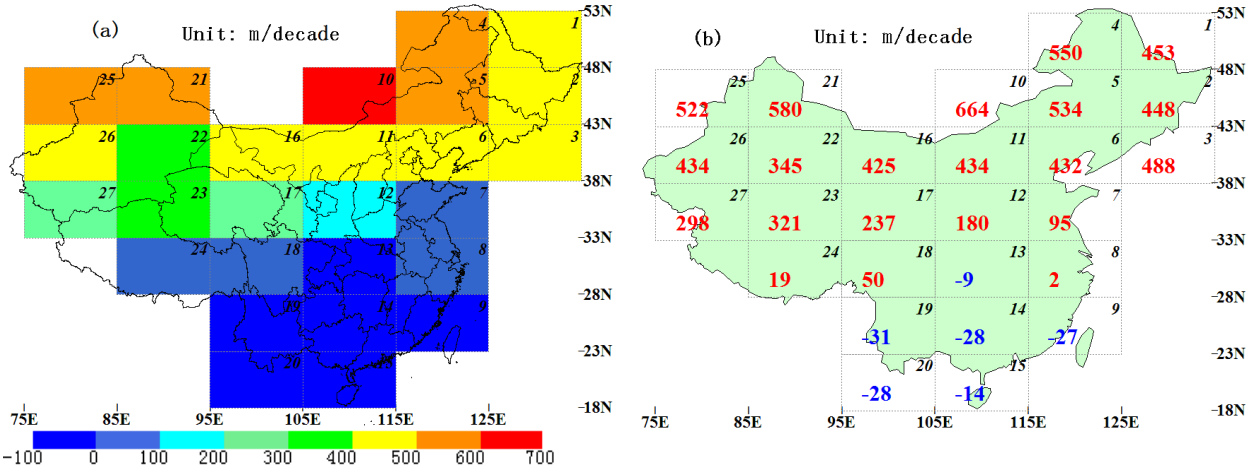

Figure 12. Maps of the 10-year-change-rate for H-CPT in each grid over 1979—2014. (a) Contour interval is 100m/decade; (b) The numerical value are the 10-year-change-rate, positive in red and negative in blue. Each lattice is signed with the digital number on the top right corner.

As shown in Fig.12, the change rate of H-CPT shows obviously spatial distribution

characteristics. From Fig.12a, under the same longitude zone with every 5° intervals, the change gradient of H-CPT decreases gradually from high latitude to low latitude over the whole China region. Under the same latitude zone with every 5° intervals, the change gradient of H-CPT increases gradually from high longitude (east area) to low longitude(west area) in the area of 95°E—135°E, 18°N—53°N (except for grid 13). In conjunction with Fig.12b, besides grid 13 which is located in Sichuan Basin region, the H-CPT of all lattices is uplift trend between 28°N —53°N latitude region, and corresponding the H-CPT of all lattices is decline trend between 18°N—28°N latitude region. The decline trend of H-CPT at low latitude has not been reported in the previous literature. The maximum uplifting rate 664m/decade occurs in grid 10 which is located at Inner Mongolia Plateau region.

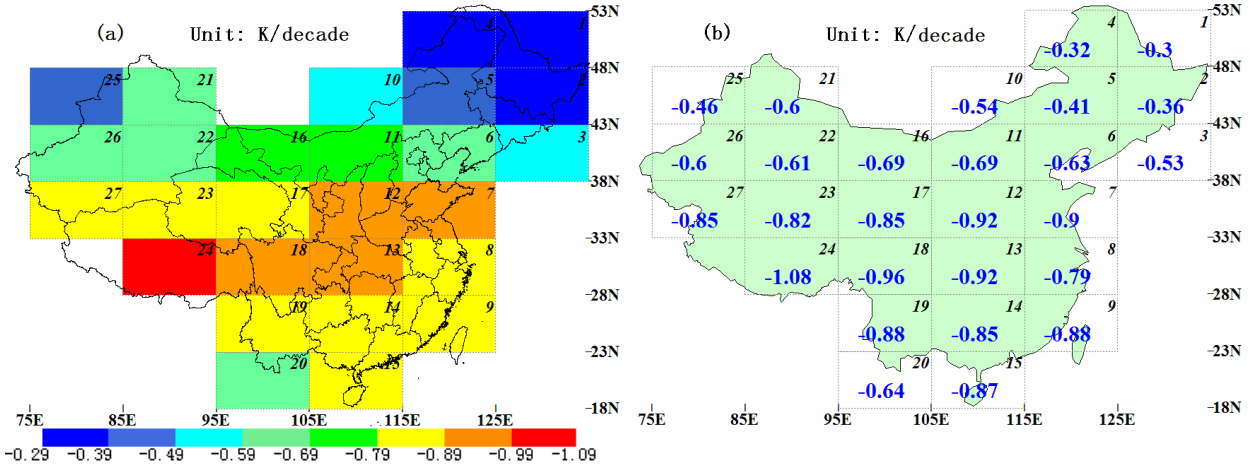

Figure 13. Maps of the 10-year-change-rate for T-CPT in each grid over 1979—2014. (a) Contour interval is 0.1K/decade; (b) The numerical value are the 10-year-change-rate, positive in red and negative in blue. Each lattice is signed with the digital number on the top right corner.

As shown in Fig.13, the change rate of T-CPT shows obviously spatial distribution characteristics. From Fig.13a, under the same longitude zone with every 5° intervals, the change gradient of T-CPT increases gradually from high latitude to low latitude in the area of 75°E—135°E, 33°N—53°N, and corresponding the change gradient of T-CPT decreases gradually from high latitude to low latitude in the area of 75°E—135°E, 18°N—33°N. In conjunction with Fig.13b, under the same latitude zone with every 5° intervals, the change rate of T-CPT increases gradually from high longitude to low longitude in the area of 28°N—53°N,95°E—135°E (except for grid 17). The T-CPT of all lattices has a cooling trend over the whole China region, the maximum cooling rate -1.08K/decade occurs in grid 24, which is located at Qinghai-Tibet Plateau region.

3.4. The annual fluctuation of the CPT properties over China during 2014

For further discussion to spatial (latitude—longitude) structure of annual variation of the CPT properties, we will focus on the annual statistics of CPT properties using 2014 year's data in following section. The H-CPT (T-CPT) is analyzed using the standard deviation method for each grid cell. The spatial distribution of the fluctuation of H-CPT and T-CPT are obtained. Fig.14 shows the average of H-CPT and T-CPT for each grid during 2014. Fig.15 shows the standard deviations of H-CPT and T-CPT for each grid during 2014.

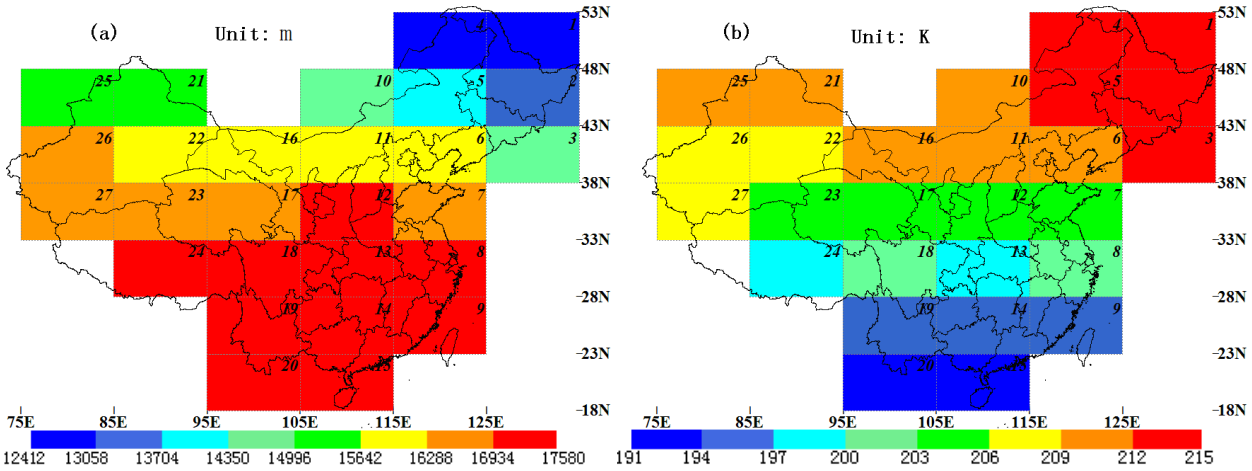

Figure 14. Maps of the average H-CPT and T-CPT in each grid during 2014:
(a) Contour interval is 646m for H-CPT; (b) Contour interval is 3K for T-CPT.

As shown in Fig.14, the average of H-CPT and T-CPT show obviously spatial distribution characteristics over China. From Fig.14a, under the same longitude zone with every 5° intervals, the average value gradient of H-CPT increases gradually from high latitude to low latitude in the whole China region. Under the same latitude zone with every 5° intervals, the average value gradient of H-CPT increases gradually from high longitude (east) to low longitude(west) in the whole China region(except for grid 12). The maximum average of H-CPT (~17.5km) occurs in low latitude zones, and the minimum average of H-CPT (~12.5km) occurs in high latitude zones. From Fig.14b, under the same longitude zone with every 5° intervals, the average value gradient of T-CPT decreases gradually from high latitude to low latitude in the whole China region. Under the same latitude zone with every 5° intervals, the average value gradient of T-CPT decreases gradually from high longitude (east) to low longitude(west) in the whole China region(except for grid 18 and grid 27). The maximum average of T-CPT (~214K) occurs in high latitude zones, and the minimum average of T-CPT (~191K) occurs in low latitude zones.

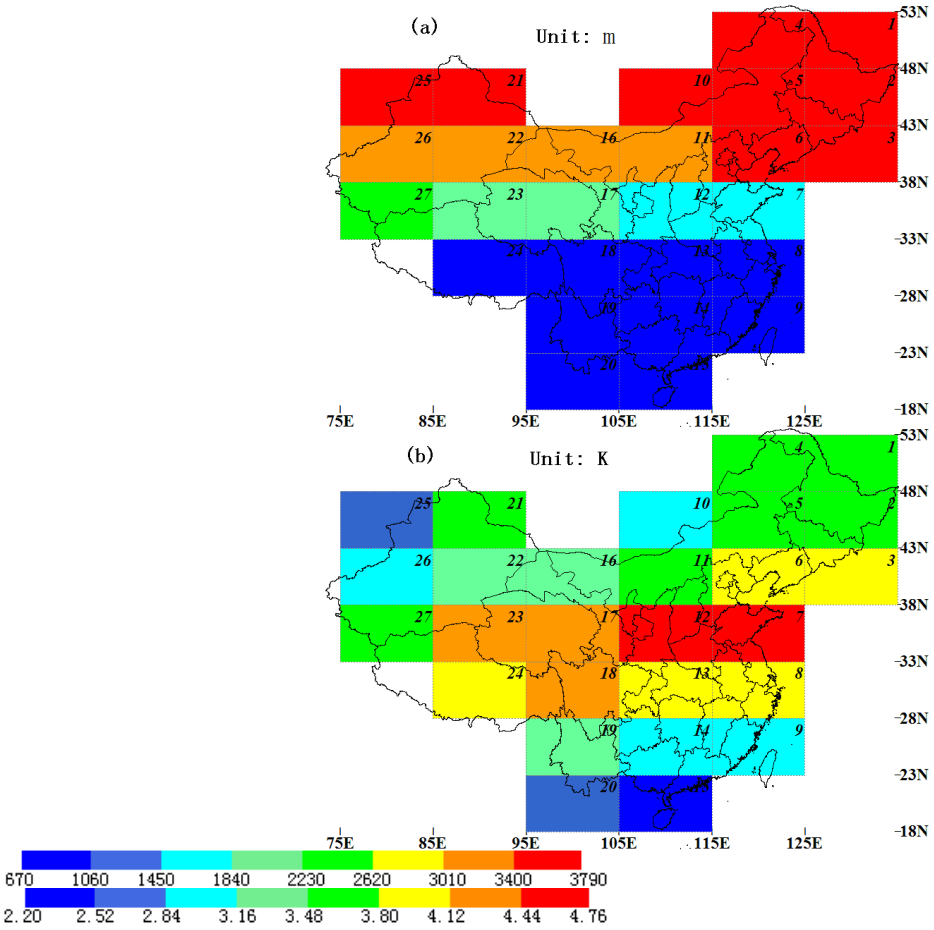

Figure 15. Maps of the standard deviations for H-CPT and T-CPT in each grid during 2014: (a) Contour interval is 390m for H-CPT; (b) Contour interval is 0.32K for T-CPT.

As shown in Fig.15, the standard deviation of H-CPT and T-CPT show obviously spatial distribution characteristics. From Fig.15a, under the same longitude zone with every 5° intervals, the standard deviation gradient of H-CPT decreases gradually from high latitude to low latitude in the whole China region. Under the same latitude zone with every 5° intervals, the standard deviation gradient of H-CPT decreases gradually from high longitude (east) to low longitude (west) within 38°N—43°N latitude zone, and corresponding the standard deviation gradient of H-CPT increases gradually from high longitude (east) to low longitude (west) within 33°N—38°N latitude zone. The maximum standard deviations of the H-CPT (~3.5km) occur in high latitude zones, and the minimum standard deviations of the H-CPT (~0.7km) occur in low latitude zones. From Fig.15b, under the same longitude zone with every 5° intervals, the standard deviations gradient of T-CPT decreases gradually from the middle latitude zone(33°N—38°N) to both sides, and the largest fluctuation of T-CPT is just in line with the rapid development economic belt of China. Under the same latitude zone with every 5° intervals, the standard

deviations gradient of T-CPT decreases gradually from high longitude (east) to low longitude (west) within 33°N—53°N latitude zones (except for grid 21), and corresponding the standard deviation gradient of T-CPT increases gradually from high longitude (east) to low longitude (west) within 18°N—33°N latitude zones(except for grid 24). The maximum standard deviations of the T-CPT (~4.7K) occur in 33°N—38°N latitude zone, and the reason may be related with the rapid developing industry in the latitude zone. The reason is worth of further investigations.

4. Conclusions

The first long-term changing trends of height and temperature of Cold-Point Tropopause were presented through analyzing the sounding dataset of 77 stations in the IGRA2 over China region from 1979 to 2014 in this study. The analysis also includes the latitudinal and longitudinal distribution, seasonal cycle, annual fluctuation, and long-term 10-year-linear-change-rate of H-CPT and T-CPT.

A total number of 1,703,696 sounding profiles were applied for this period. By using the least squares regression method, The 10-year-linear-change-rate of the average temperature and height of CPT were obtained. it is found that the H-CPT increases approximately at a mean rate of 273m/decade, and overall significant cooling rate of -0.70K/decade for T-CPT in the whole China region. Especially, the summer's CPT is located highest and coldest than the other seasons' over the whole China, and the uplift of the H-CPT in China region is mainly due to the uplift during winter and spring. Through the analysis for the latitude distribution of long-term trends of the CPT properties, it is found that the change rates (even the change direction) of H-CPT and T-CPT show obviously latitude distribution characteristics. The H-CPT is uplift trend between 28°N—53°N latitude region with the change rates vary from the minimum 4m/decade in 28°N—33°N latitude zone to 499m/decade in 48°N—53°N latitude zone. The H-CPT has decline trend between 18°N—23°N latitude zone with -19m/decade and between 23°N—28°N latitude zone with -29m/decade. The T-CPT has an overall cooling trend for all latitude zones, and the change rates of T-CPT vary from -0.8/decade in 18°N—23°N latitude zone to the minimum -0.32K/decade in 48°N—53°N latitude zone.

The following phenomena were not reported in previous literature: the H-CPT has decline trend with a negative change rate at low latitude region; the difference of H-CPT is becoming smaller between high latitude and low latitude year by year, and the difference of T-CPT is

becoming larger between high latitude and low latitude.

Through the analysis for the spatial (latitude-longitude) structure of long-term trends of the CPT properties for each grid cell, it is found that the change rates of H-CPT(T-CPT) present obviously spatial distribution characteristics: the 10-year-change-rate is not only significantly dependent on latitude, but also dependent on longitude, the maximum uplifting rate 664m/decade occurs in Inner Mongolia Plateau region, and the maximum cooling rate -1.08K/decade occurs in Qinghai-Tibet Plateau region. As for the reasons for these changes and the change rates are worthy of further studies.

The spatial structure of annual fluctuation of H-CPT(T-CPT) is analyzed for each grid using the standard deviation method, it is found that the annual fluctuation of T-CPT(T-CPT) present obviously spatial distribution characteristics. The maximum standard deviations of the T-CPT (~4.7K) occur in 33°N—38°N latitude zone, and the standard deviations of T-CPT decreases gradually from the middle latitude zone(33°N—38°N) to both sides. Just in line with the rapid development economic belt of China. The reason is worth of further investigations.

ACKNOWLEDGEMENTS

We would like to thank National Oceanic and Atmospheric Administration (NOAA) for supplying the beta release of version 2 of the Integrated Global Radiosonde Archive(IGRA2) dataset. This work is funded by the National Natural Science Foundation of China (51104003, 41505023, 61077081).

References

Anthes, R. A., et al. (2008), The COSMIC/FORMOSAT-3 Mission: Early Results, Bulletin of the American Meteorological Society, 89, 313, doi:10.1175/BAMS-89-3-313.

Austin, J., and T. J. Reichler (2008), Long-term evolution of the cold point tropical tropopause: Simulation results and attribution analysis, J. Geophys. Res., 113, D00B10, doi:10.1029/2007JD009768.

Durre, I. (2014), Integrated Global Radiosonde Archive (IGRA) V2beta Readme File[OL], Available: http://www1.ncdc.noaa.gov/pub/data/igra/v2beta/igra2-readme.txt

Durre, I., R. S. Vose, and D. B. Wuertz (2006), Overview of the integrated global radiosonde archive, J. Climate, 19(1), 53—68, doi:10.1175/JCLI3594.1.

Durre, I., R. S. Vose, and D. B. Wuertz (2008), Robust automated quality assurance of

radiosonde temperatures, J. Appl. Meteorol. Climatol., 47(8), 2081—2095, doi:10.1175/2008JAMC1809.1.

Feng, S., Y. Fu, and Q. Xiao (2012), Trends in the global tropopause thickness revealed by radiosondes, Geophys. Res. Lett., 39, L20706, doi:10.1029/2012GL053460.

Joowan, K, and S.W.Son (2012), Tropical Cold-Point Tropopause: Climatology, Seasonal Cycle, and Intraseasonal Variability Derived from COSMIC GPS Radio Occultation Measurements, J. Climate, 25(8), 5343—5360, doi:10.1175/JCLI-D-11-00554.1

Kim, J., K. M. Grise, and S.-W. Son (2013), Thermal characteristics of the cold-point tropopause region in CMIP5 models, J. Geophys. Res. Atmos., 118, 8827—8841, doi:10.1002/jgrd.50649

Kim, J.-E., and M. J. Alexander (2015), Direct impacts of waves on tropical cold point tropopause temperature, Geophys. Res. Lett., 42, 1584—1592,doi:10.1002/2014GL062737.

Son, S.-W., N. F. Tandon, and L. M. Polvani (2011), The fine-scale structure of the global tropopause derived from COSMIC GPS radio occultation measurements, Journal of Geophysical Research (Atmospheres), 116, D20113, doi:10.1029/2011JD016030.

Xian, T., and Y. Fu (2015), Characteristics of tropopause-penetrating convection determined by TRMM and COSMIC GPS radio occultation measurements. J. Geophys. Res. Atmos., 120, 7006–7024. doi: 10.1002/2014JD022633.

Xie, F., Li, J.P., Tian, W.S., Li, Y.J. & Feng, J(2014). Indo-Pacific Warm Pool Area Expansion,Modoki Activity, and Tropical Cold-Point Tropopause Temperature Variations. Sci. Rep. 4, 4552; doi:10.1038/srep04552.

Xu X H, Gao P, Zhang X H (2013). Structure and variation of the tropopause over China with COSMIC radio occultation bending angles. Chinese J.Geophys.(in Chinese), 56(8):2531-2541,doi:10.6038/cjg20130804.

Zhou, X., M. A. Geller, and M. Zhang(2001a), Tropical cold point tropopause characteristics derived from ECMWF reanalyses and soundings. J. Climate, 14, 1823—1838. doi: 10.1175/1520-0442(2001)014<1823:TCPTCD>2.0.CO;2

Zhou, X., M. A. Geller, and M. Zhang (2001b): Cooling trend of the tropical cold point tropopause temperatures and its implications. J. Geophys. Res., 106, 1511—1522. doi: 10.1029/2000JD900472

Figure Captions

Figure 1. The flow chart of the quality control for the CPT data preprocess: to obtain an effective H-CPT and T-CPT.

Figure 2. Examples of the CPT data quality control process: three sounding profiles are at 1200 UTC in Beijing (stationID: CHM00054511).

Figure 3. The distribution of available data in China for each year from 1956 to 2014. (a) Number of sounding stations for each year where data are available before CPT quality control process (black triangle) and after CPT quality control process (red star). (b) Number of total sounding profiles for each year where data are available before CPT quality control process (black triangle) and after CPT quality control process (red star).

Figure 4. The distribution of H-CPT and T-CPT of 1,703,969 soundings after the abnormal-value-remove. (a) Number of total profiles of H-CPT for each integer height interval. (b) Number of total profiles of T-CPT for each integer temperature interval.

Figure 5. The spatial division and geographic distribution of the 77 stations over China: the red stars mark the location of S77, the blue digital on center in each grid represents the station count of the grid containing, the black digital on the top right corner in each grid represents the number of the grid.

Figure 6. The average variability in height and temperature of CPT. The solid lines are the corresponding linear trends during 1979—2014 with a least square procedure. The change rates are shown at the right-top of each diagram. (a)The annual-mean trends of H-CPT; (b) The annual-mean trends of T-CPT; (c) The seasonal-mean trends of H-CPT; (d)The seasonal-mean trends of T-CPT.

Figure 7. Latitudinal distribution of the annual-mean trends for CPT with the interval of 5° during 1979—2014. (a)The annual-mean trends of H-CPT with respect to soundings in each latitude zone; (b) The annual-mean trends of T-CPT with respect to soundings in each latitude zone; (c) Latitudinal distribution of the 10-year-change-rate for H-CPT; (d) Latitudinal distribution of the 10-year-change-rate for T-CPT.

Figure 8. Latitudinal distribution of the seasonal-mean trends for H-CPT in each latitude zone during 1979—2014; (a) Winter; (b) Spring; (c) Summer; (d) Autumn.

Figure 9. Latitudinal distributions of the 10-year-change-rate of H-CPT with the interval of 5° for four seasons .

Figure 10. The latitudinal distribution of the seasonal-mean trends for T-CPT in each latitude zone during 1979—2014; (a) Winter; (b) Spring; (c) Summer; (d) Autumn.

Figure 11. The latitudinal distribution of the 10-year-change-rate of T-CPT with the interval of 5° for four seasons.

Figure 12. Maps of the 10-year-change-rate for H-CPT in each grid over 1979—2014. (a) Contour interval is 100m/decade; (b) The numerical value are the 10-year-change-rate, positive in red and negative in blue. Each lattice is signed with the digital number on the top right corner.

Figure 13. Maps of the 10-year-change-rate for T-CPT in each grid over 1979—2014. (a) Contour interval is 0.1K/decade; (b) The numerical value are the 10-year-change-rate, positive

in red and negative in blue. Each lattice is signed with the digital number on the top right corner.

Figure 14. Maps of the average H-CPT and T-CPT in each grid during 2014: (a) Contour interval is 646m for H-CPT; (b) Contour interval is 3K for T-CPT.

Figure 15. Maps of the standard deviations for H-CPT and T-CPT in each grid during 2014: (a) Contour interval is 390m for H-CPT; (b) Contour interval is 0.32K for T-CPT.

Figures.

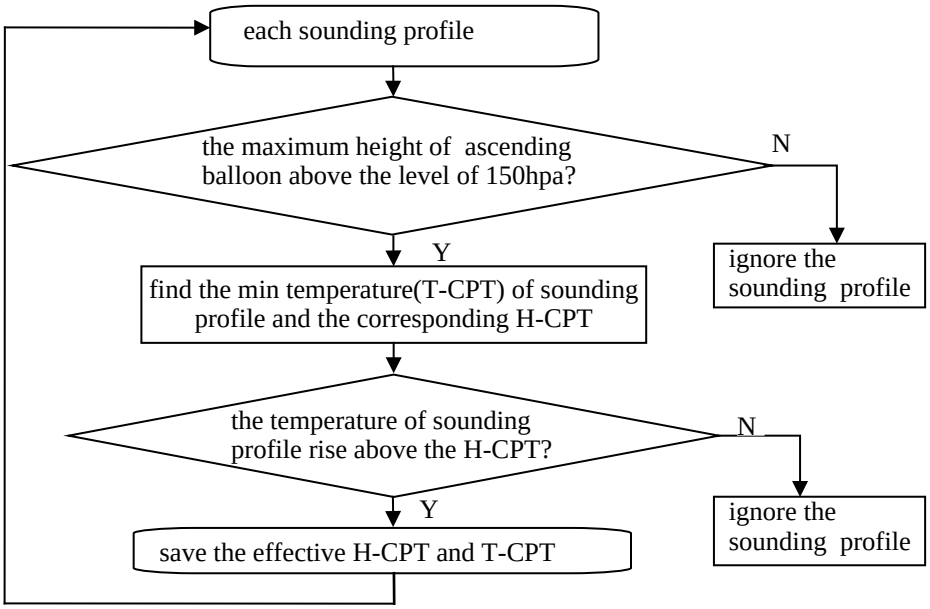

Figure 1. The flow chart of the quality control for the CPT data preprocess: to obtain an effective H-CPT and T-CPT

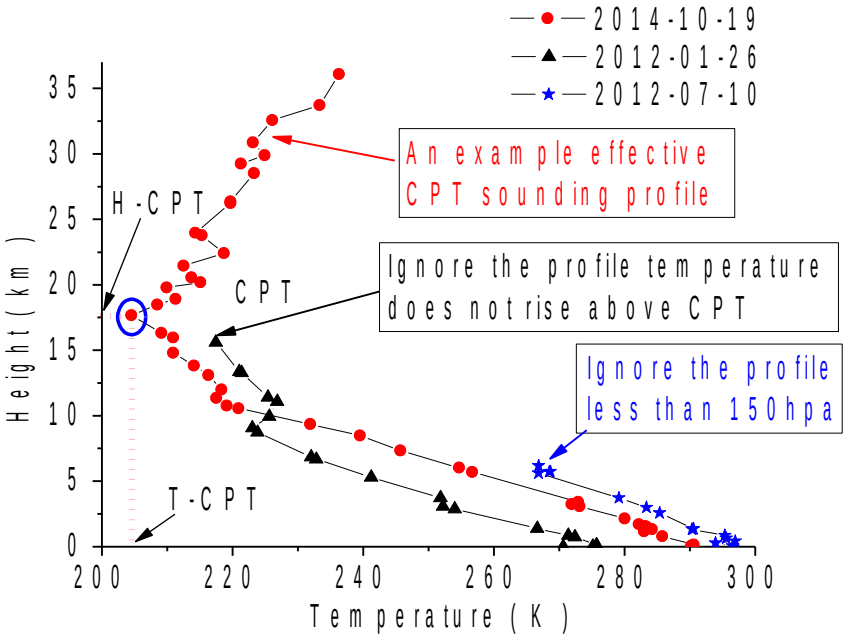

Figure 2. Examples of the CPT data quality control process: three sounding profiles are at 1200 UTC in Beijing (stationID: CHM00054511)

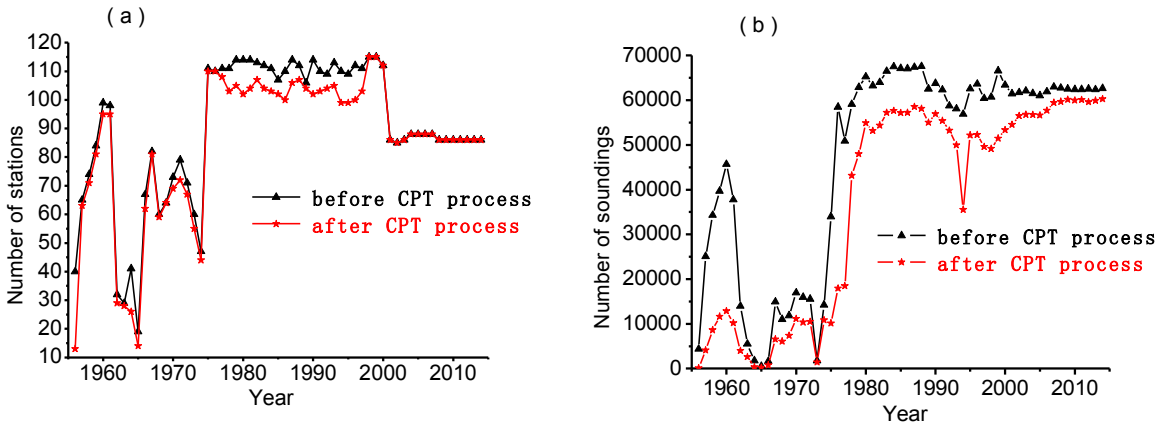

Figure 3. The distribution of available data in China for each year from 1956 to 2014. (a) Number of sounding stations for each year where data are available before CPT quality control process (black triangle) and after CPT quality control process (red star). (b) Number of total sounding profiles for each year where data are available before CPT quality control process (black triangle) and after CPT quality control process (red star).

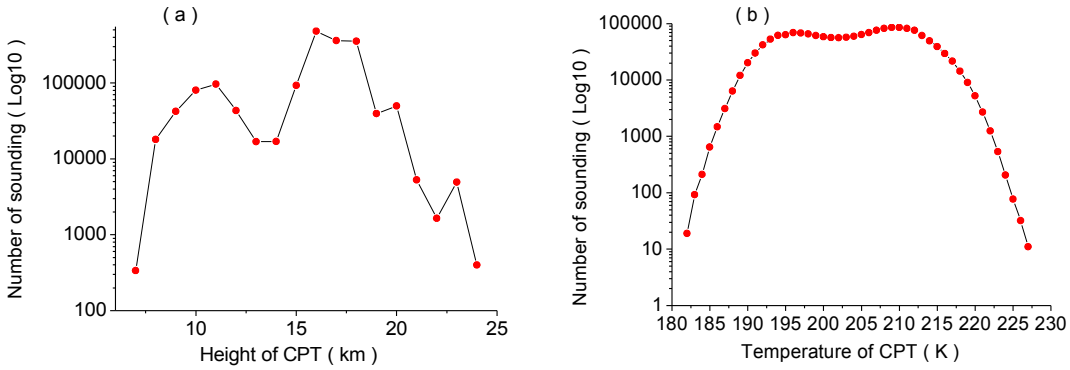

Figure 4. The distribution of H-CPT and T-CPT of 1,703,969 soundings after the abnormal-value-remove. (a) Number of total profiles of H-CPT for each integer height interval. (b) Number of total profiles of T-CPT for each integer temperature interval.

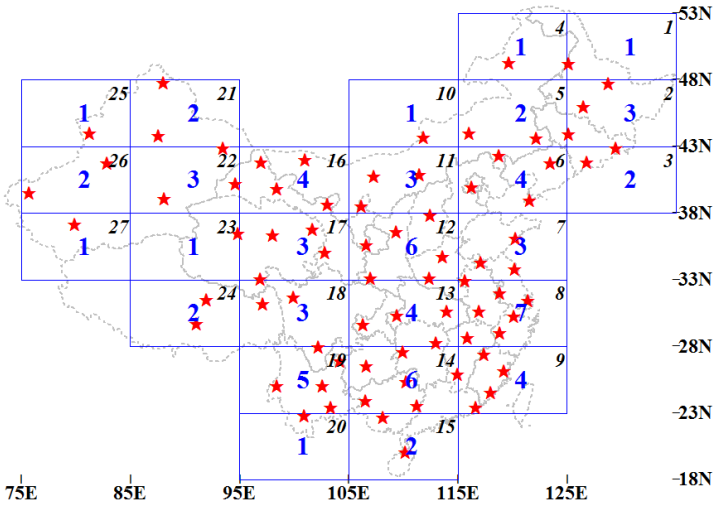

Figure 5. The spatial division and geographic distribution of the 77 stations over China: the red stars mark the location of S77, the blue digital on center in each grid represents the station count of the grid containing, the black digital on the top right corner in each grid represents the number of the grid

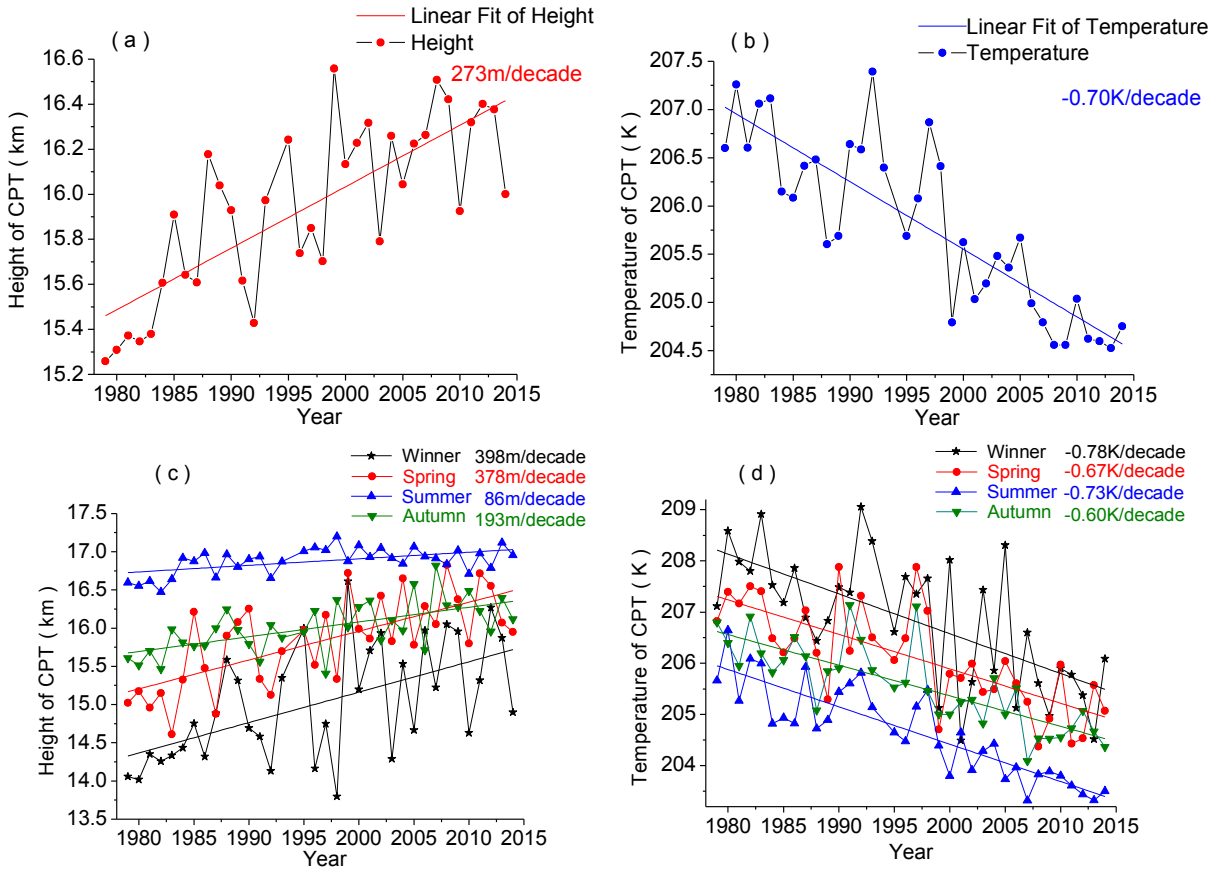

Figure 6. The average variability in height and temperature of CPT. The solid lines are the corresponding linear trends during 1979—2014 with a least square procedure. The change rates are shown at the right-top of each diagram. (a)The annual-mean trends of H-CPT; (b) The annual-mean trends of T-CPT; (c) The seasonal-mean trends of H-CPT; (d)The seasonal-mean trends of T-CPT.

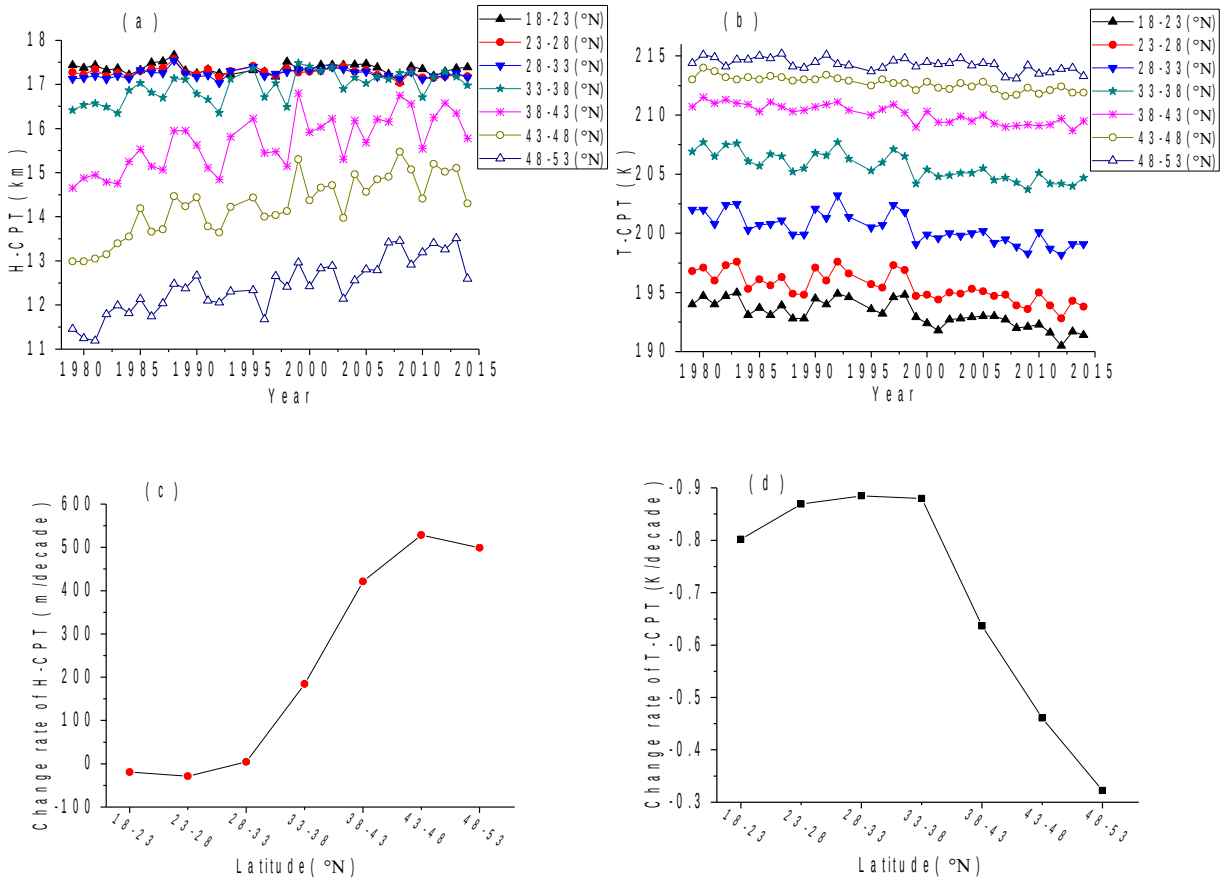

Figure 7. Latitudinal distribution of the annual-mean trends for CPT with the interval of 5° during 1979—2014. (a)The annual-mean trends of H-CPT with respect to soundings in each latitude zone; (b) The annual-mean trends of T-CPT with respect to soundings in each latitude zone; (c) Latitudinal distribution of the 10-year-change-rate for H-CPT; (d) Latitudinal distribution of the 10-year-change-rate for T-CPT

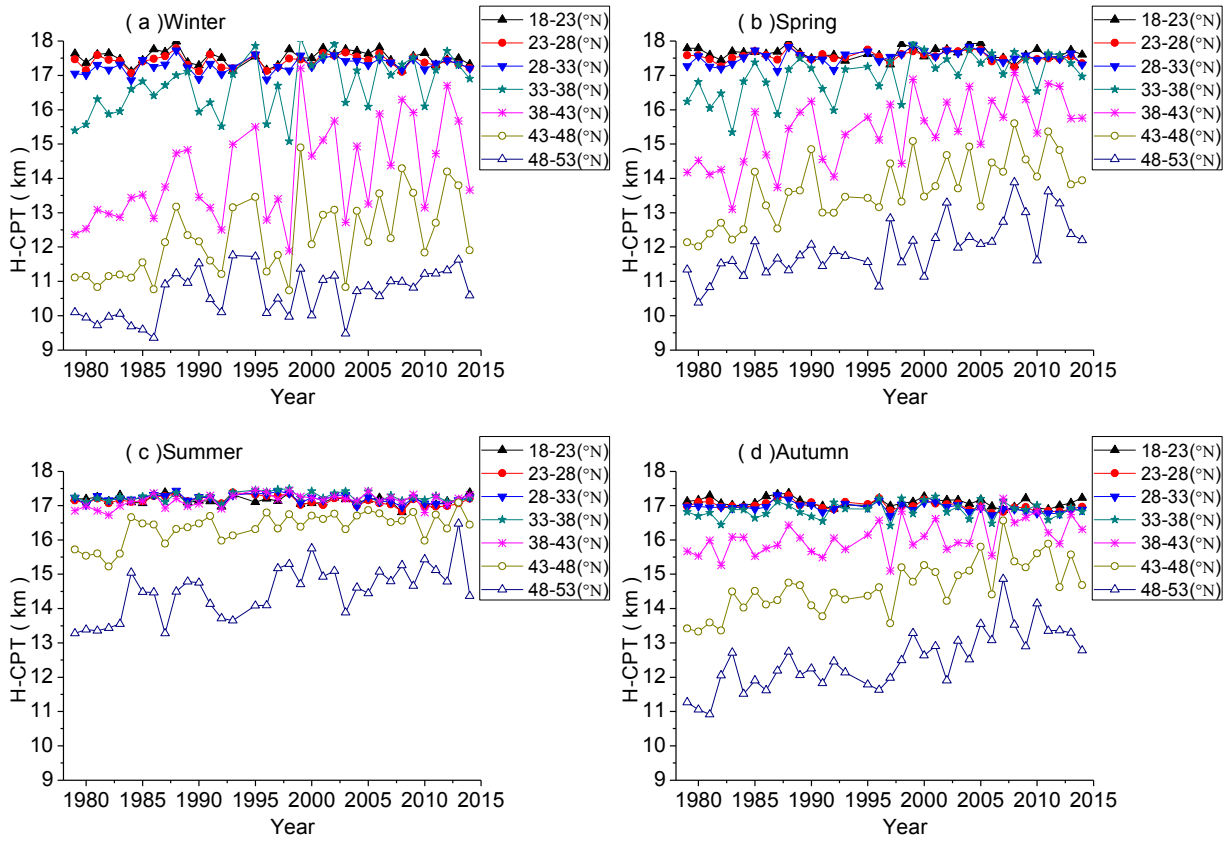

Figure 8. Latitudinal distribution of the seasonal-mean trends for H-CPT in each latitude zone during 1979—2014; (a) Winter; (b) Spring; (c) Summer; (d) Autumn

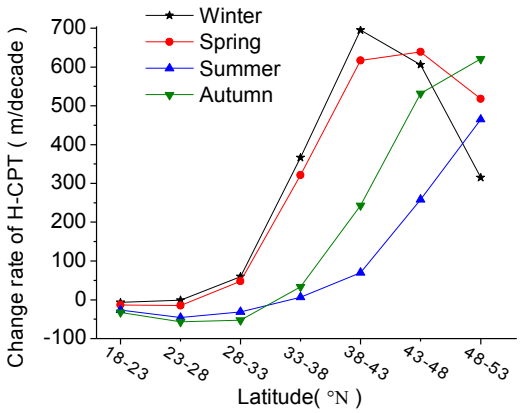

Figure 9. Latitudinal distributions of the 10-year-change-rate of H-CPT with the interval of 5° for four seasons

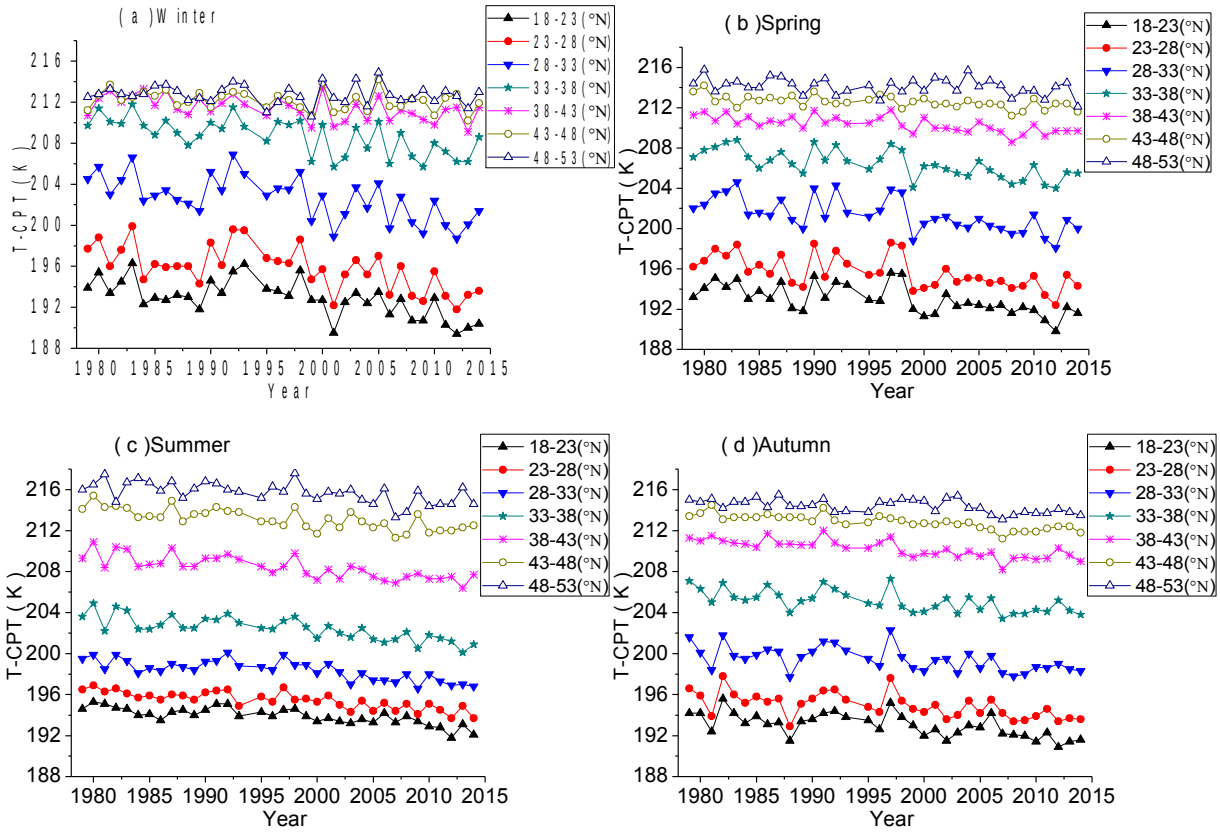

Figure 10. The latitudinal distribution of the seasonal-mean trends for T-CPT in each latitude zone during 1979—2014; (a) Winter; (b) Spring; (c) Summer; (d) Autumn

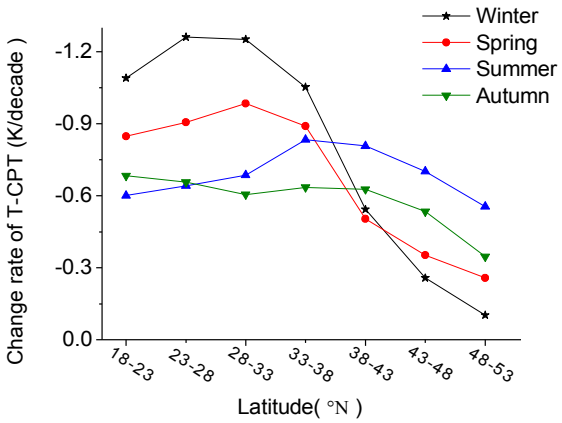

Figure 11. The latitudinal distribution of the 10-year-change-rate of T-CPT with the interval of 5° for four seasons

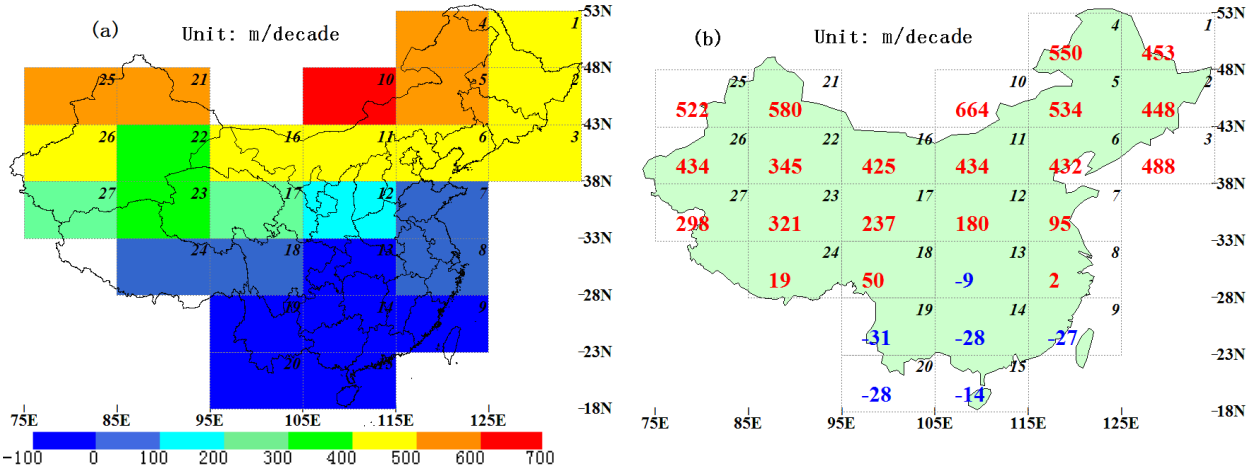

Figure 12. Maps of the 10-year-change-rate for H-CPT in each grid over 1979—2014. (a) Contour interval is 100m/decade; (b) The numerical value are the 10-year-change-rate, positive in red and negative in blue. Each lattice is signed with the digital number on the top right corner.

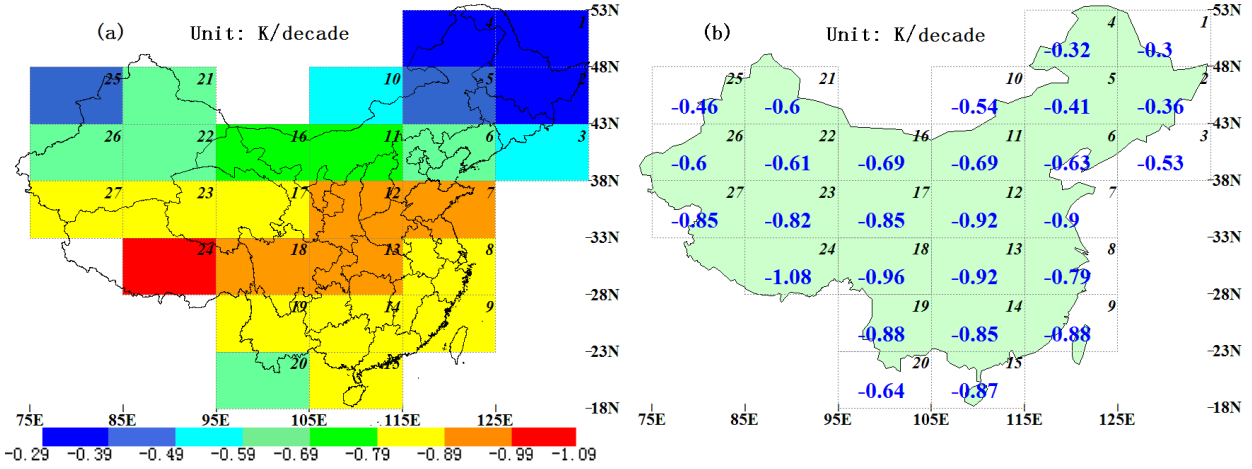

Figure 13. Maps of the 10-year-change-rate for T-CPT in each grid over 1979—2014. (a) Contour interval is 0.1K/decade; (b) The numerical value are the 10-year-change-rate, positive in red and negative in blue. Each lattice is signed with the digital number on the top right corner.

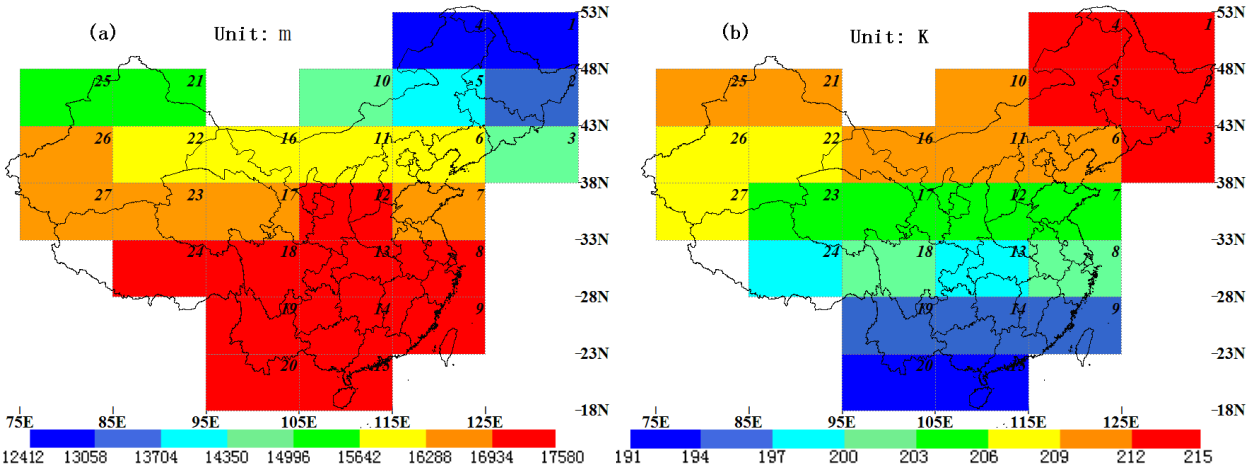

Figure 14. Maps of the average H-CPT and T-CPT in each grid during 2014: (a) Contour interval is 646m for H-CPT; (b) Contour interval is 3K for T-CPT.

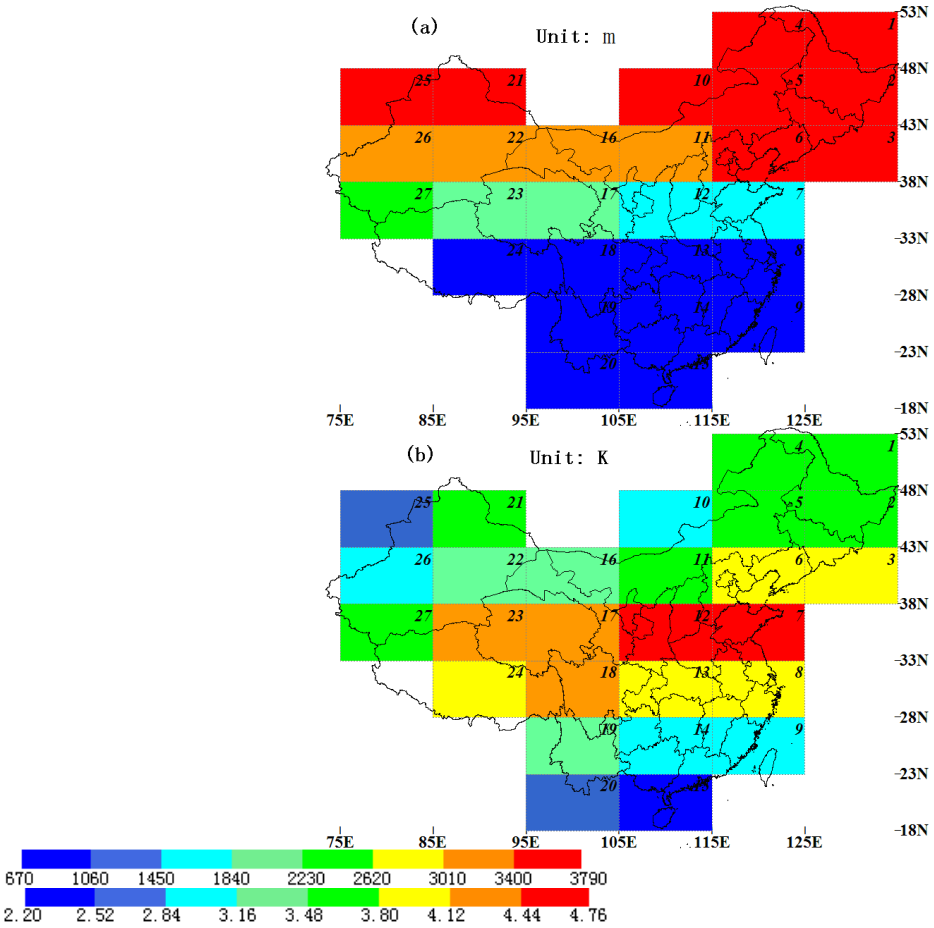

Figure 15. Maps of the standard deviations for H-CPT and T-CPT in each grid during 2014:

(a) Contour interval is 390m for H-CPT; (b) Contour interval is 0.32K for T-CPT.